IN-29-CR
26172
P. 174

GASCAN II
PAYLOAD INTEGRATION

by:

Henry B. Brown, Jr.
Jared G. Buzby
Barbara J. Doyle
Benedict C. Wibisono

Advised by:

Prof. Robert C. Labonte
Prof. Joseph J. Rencis

Report Submitted to:
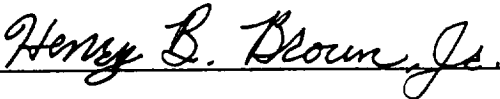
ADVANCED SPACE DESIGN PROGRAM

In Cooperation with:

The **MITRE** Corporation

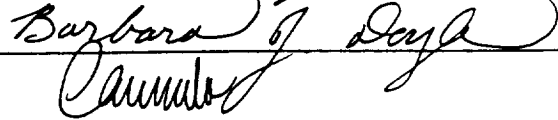GASCAN II PAYLOAD INTEGRATION

BY:

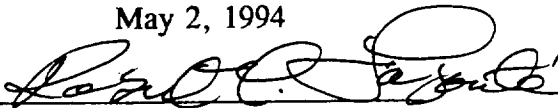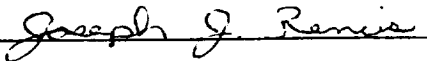Henry B. Brown, Jr.

Jared G. Buzby

Barbara J. Doyle

Benedict C. Wibisono

May 2, 1994

Prof. Robert C. Labonte, Advisor

Prof. Joseph J. Rencis, Advisor

This project is submitted in partial fulfillment of the Bachelor of Science degree requirements of Worcester Polytechnic Institute. The views and opinions expressed herein are those of the authors and do not necessarily reflect the positions or opinions of Program Sponsors or Worcester Polytechnic Institute.

This report is the product of an educational program, and is intended to serve as partial documentation for the evaluation of academic achievement. The report should not be construed as a working document.

ABSTRACT

This MQP is an ongoing part of the NASA Advanced Space Design Program which examines the integration of the WPI/MITRE Get Away Special Canister (GASCan II). GASCan II contains the Ionospheric Properties and Propagation, Micro-Gravity Ignition, and Rotational Fluid Flow experiments, as well as the Integrated Support Structure. The objectives this year were to finalize the power supply system, connections for experiments, mechanical design of the IPPE's antenna and to update the structural and vibrational analyses of the Integrated Support Structure.

ACKNOWLEDGEMENTS

TABLE OF CONTENTS

AUTHORSHIP PAGE

LIST OF FIGURES

LIST OF TABLES

EXECUTIVE SUMMARY

The Mitre Corporation of Bedford, MA, donated a Get Away Special canister (GASCan) to the WPI Advanced Space Design Program. The purpose of this GASCan is to conduct experiments aboard the space shuttle in a micro-gravity environment. With the combined support of Mitre and NASA/USRA, students can design and create micro-gravity experiments, which will fly aboard the space shuttle in this GASCan.

GASCan II consists of three experiments: the Ionospheric Propagation Properties experiment (IPPE), the Micro-gravity Ignition experiment (MGI), and the Rotational Fluid Flow experiment (RFF). The objective of this project is to design, analyze, and integrate the structure and components of GASCan II in accordance with the structural and vibrational requirements of NASA.

This project is in the sixth year of a seven year development process to produce flight-ready hardware, which began in 1988. The first MQP group produced an initial design of the integrated support structure. The second MQP group delivered a preliminary support structure design, a preliminary structural and vibrational ANSYS analysis of the support structure, and a list of recommendations for payload integration. The third MQP group developed a preliminary design for the battery box and reanalyzed the structural and vibrational integrity of the GAScan. The fourth MQP conducted analyses on the support structure. The 1992-93 group completed a design of the battery box, and verified the structural and vibrational integrity of the integrated support structure (ISS). This year the ISS group became the Payload Integration team, responsible not only for the structural aspects of the GASCan, but for the integration of all experiments

and the wiring and connections between all components.

The 1992-1993 ISS team designed a battery box; however, due to spacial and wiring issues, the battery box was redesigned by this year's Integration team. This battery box was also designed to exceed the NASA, GATES Energy Products, and Advanced Space Design specifications. This design also reflects the change in venting requirements for batteries.

Another major concern of this year's Integration team was the design of the IPPE antenna. While the antenna has been an issue for the GASCan II project for many years, only the electrical requirements were studied. Therefore, this year's team needed to examine the structural design. Since the antenna is outside the GASCan, stringent structural and vibrational requirements are necessary for the antenna to maintain structural integrity and pass NASA safety requirements. Therefore, an antenna was designed that successfully met all necessary structural and vibrational requirements, both through finite element analysis and hand calculations.

The next issue to be addressed concerned the structural and vibrational analyses of the support structure using the finite element method. A finite element model of the ISS was developed by last year's ISS team, and was updated by this year's team, reflecting all changes in hardware. Hand calculations were also performed to verify the IMAGES-3D commercial software package representation. The structural analysis achieved positive margins-of-safety under the inertial loading cases required by the NASA. The fundamental frequency was greater than that required by NASA for the vibrational analysis. These analyses indicate that the support structure satisfies the safety

criteria set forth by NASA.

1.0. OBJECTIVES

The main responsibility of the GASCan II Payload Integration team is to design an Integrated Support Structure (ISS) that will house the three experiments and their power supplies while satisfying all NASA requirements for safety and minimizing risk of experiment failure. The main objectives of the 1993-94 Payload Integration team are the design of individual components, their connections to the structure and verification of the structural integrity of GASCan II.

The Payload Integration team designed several new components for the ISS including the battery box, lateral bumpers, IPPE antenna and MGI canister mounting brackets. The battery box design from the 1992-93 MQP was modified to accommodate spacial considerations. The Integration team also designed an IPPE antenna to satisfy functionality and structural integrity requirements. The MGI canister mounting brackets were designed by the team to attach the MGI canisters to the tri-wall structure. The team designed a lateral bumper that incorporates a working geometric design with realistic safety locking procedures to prevent the bumpers from possible in-flight loosening.

The finite element model of the Integrated Support Structure was updated and reanalyzed. This was used to verify the structural integrity of the ISS under the loads it will encounter during flight. Analytical calculations were used to support the finite element model results.

2.0. OVERVIEW OF GASCAN II

The GASCan II is a payload package that will carry three experiments aboard the space shuttle flight. The package will consist of experiments in ionospheric properties and propagation, micro-gravity ignition, and rotational fluid flow (RFF), as well as the integrated support structure (ISS) by which these experiments are structurally incorporated into a single package. Figure 2.1 shows the GASCan ISS with the experiments attached. This figure shows the key elements of GASCan II: integrated support structure (including mid-plate, tri-wall flanges, and center shaft), four (4) micro-gravity ignition canisters, battery box, rotational fluid flow experiment, and necessary computer hardware (housed on the tri-wall structure).
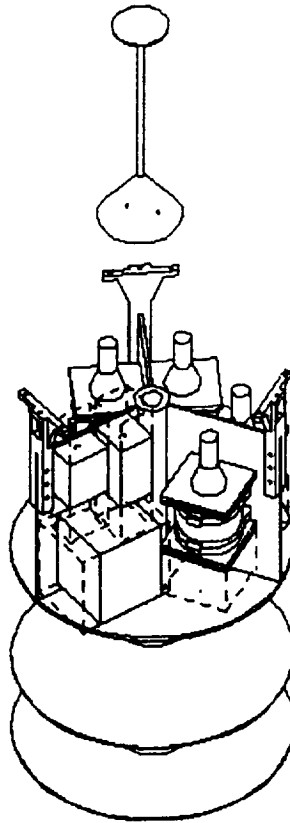
Figure 2.1 GASCan II, with experiments

Tri-wall flanges

Structure mounting
brackets

Midplate

ISS center shaft

RFF center shaft
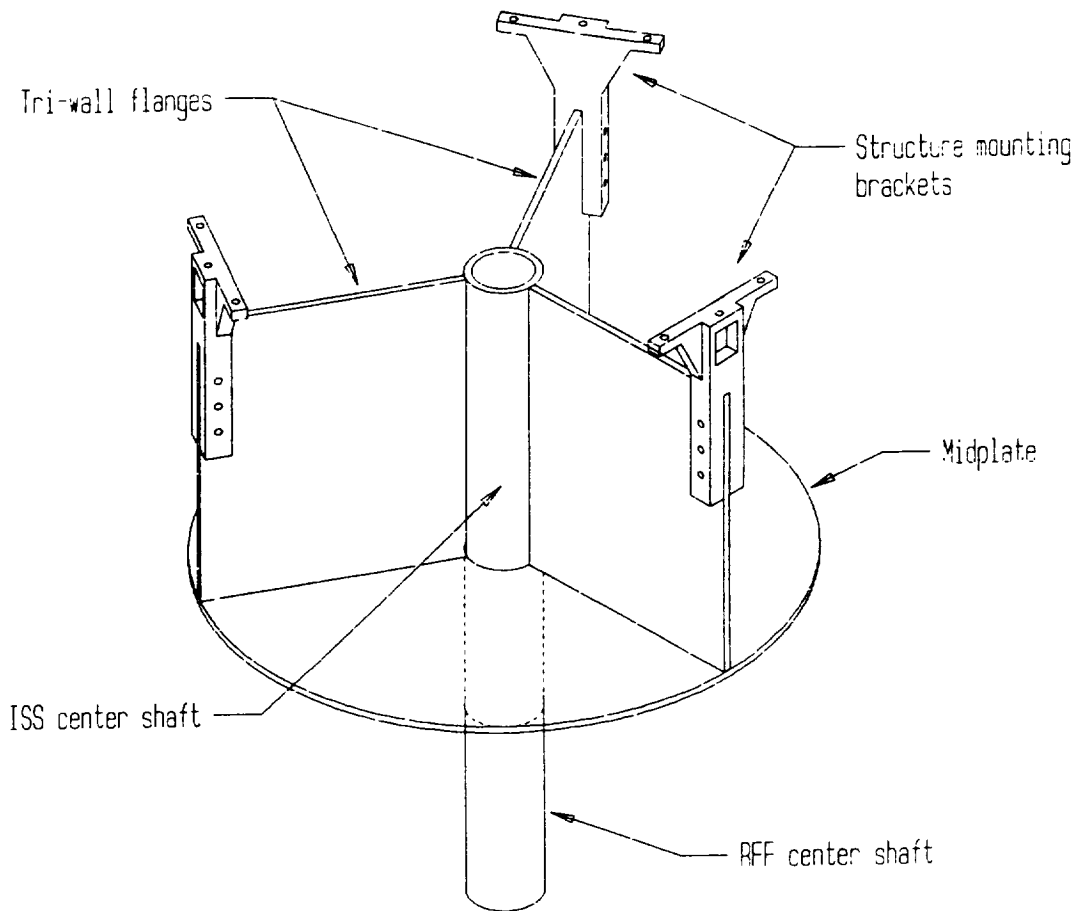
Figure 2.2 ISS structural components

2.1.4. Structure Mounting Brackets

The ISS will be mounted in the GASCan payload canister by means of three structure mounting brackets, or "legs", which are bolted to the top outer corners of the tri-wall flanges and to the canister lid.   The structure mounting brackets can be seen in Figure 2.2.

4

2.2. GASCAN EXPERIMENTS

2.2.1. Ionospheric Properties and Propagation Experiment (IPPE)

The IPPE consists of a CPU, a log electrometer, and a receiver inside the GASCan, as well as the antenna, which mounted outside the GASCan. These boxes will be mounted on the tri-wall structure as shown in Figure 2.1. The ESA probe, which was going to be mounted outside the GASCan with the antenna, has been removed. This year, special attention has been given to the antenna, due to the fact that its structural aspects had not been examined yet. Thus, the antenna is nearly completed, meeting stringent structural and vibrational requirements.

2.2.2. Micro-gravity Ignition Experiment (MGI)

The micro-gravity ignition experiment consists of four canisters, in which the energy and time required for ignition in micro-gravity will be measured, and a CPU board to control the experiment. As Figure 2.1 shows, the canisters will be mounted on two of the tri-wall flanges, two canisters on each flange, one on each side. They will be mounted using eight brackets (2 for each canister), that were designed by the 1993-94 Payload Integration team.

2.2.3. Rotational Fluid Flow in Micro-gravity (RFF)

The RFF experiment measures the rate of vortex formation in a fluid with varying gravitational constants. This experiment is mounted between two plates that are attached to the RFF center shaft. The RFF plates spin around the shaft to produce a gravitational effect in micro-gravity, and the mechanisms that allow this require that the RFF be permanently attached to the RFF shaft. Therefore, the split center shaft design was

implemented to allow removal of the RFF for easy access to the battery box.

3.0. VIBRATIONAL ANALYSIS

3.1. ANALYSIS OVERVIEW

A vibrational analysis of GASCan II was carried out using the Modal Analysis capability of IMAGES-3D, a PC based commercial finite element software package [1]. A three-dimensional finite element model was generated and the first four natural frequencies and corresponding mode shapes were determined using the Subspace Iteration Method. This analysis was conducted to fulfill NASA safety requirements [2] concerning the vibrational integrity of GASCan II.

3.2. THREE-DIMENSIONAL VIBRATIONAL ANALYSIS

3.2.1. Finite Element Model

The GASCan II finite element model consists of 1201 nodes, 990 four node quadrilateral plate elements, 180 three node triangular plate elements, 109 beam elements, and 3 linear spring elements, creating 5613 total degrees of freedom. Appendix A shows the nodal, plate and beam element numbers associated with the various components of the ISS. The material of the support structure is aluminum 6061-T6, and its mechanical properties can be found in Appendix B. The circular plates and tri-walls of the ISS are modeled with quadrilateral and triangular plate elements. Beam elements are used to model the centershaft and legs as shown in Figure 3.1. Thickness and diameter changes along the centershaft were accounted for by modifying the cross-sectional properties of the beam elements modeling the various sections of the shaft.

7
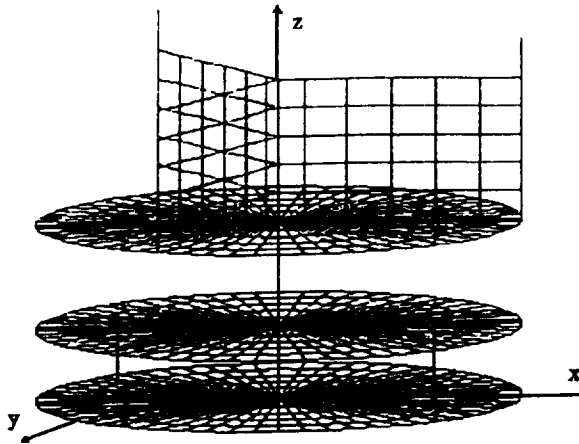
Figure 3.1 Three-dimensional model of ISS.

3.2.2. MODEL WEIGHT

The total weight of GASCan II consists of the support structure and the individual experiments. The total weight of GASCan II is currently estimated at 177.63 lbs. The weights of each component and each experiment can be found in Appendix C. Beam and plate elements were used to represent the weight of the support structure and experiments were represented by concentrated weights at nodal locations which best approximate their actual weights and locations. The values of the concentrated weights and their nodal locations can be found in Appendix D.

The Create/Edit Weights submenu option of the Modal Analysis menu in IMAGES-3D was used to create the concentrated weights. This method returned a total calculated weight of 175.70 lbs, a difference of 1.1 percent from the actual. The center of gravity returned by IMAGES-3D is stated in Appendix C. The coordinates were verified and checked against those calculated by theoretical methods. The differences

8

between the two centers of gravity is less than 0.9 percent of the ISS length along each axis. This calculation is used as a check of the model's reliability.

3.2.3. BOUNDARY CONDITIONS

The ISS is cantilevered by its legs to the GASCan mounting plate; therefore, the model has to be fully constrained in all six degrees of freedom at the nodes representing this connection as shown in Figure 3.2. The z-rotation restraints in Figure 3.2 are required to avoid a singularity solution error occurring when beam and plate elements intersect orthogonally. The beam has a rotational degree of freedom along its length while the plate element has no inplane rotational degree of freedom. The node where they connect must be restrained in the local z-rotation to suppress a local rigid body rotational mode. The lateral bumpers were modeled using linear spring elements having a stiffness of 1.25 x 10^6 lb/in, which was determined using IMAGES-3D and is in Appendix L.
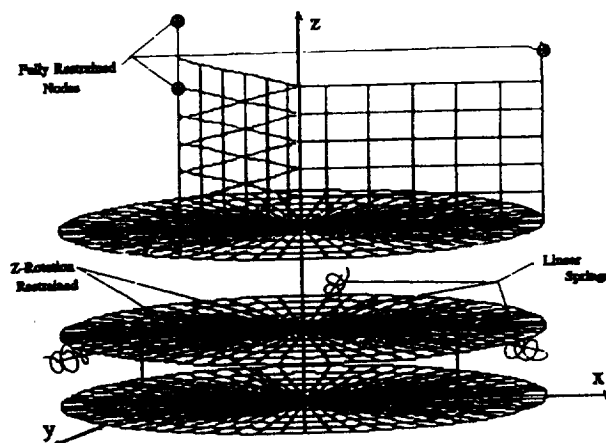
Figure 3.2 ISS nodal restraints.

9

3.3. THREE-DIMENSIONAL VIBRATIONAL ANALYSIS RESULTS

The first four natural frequencies and mode shapes for the ISS are stated in Table 3.1. The fundamental frequency of 61.39 Hz is greater than the 51 Hz required by the NASA Simplified Options for STS Payloads [4], thus verifying the vibrational integrity of the Integrated Support Structure. However, as the stiffness of the lateral bumpers have recently been updated along with some recent changes in the RFF platform configuration, a fully updated analysis will be conducted within the next month. These changes should only introduce minor changes to into the final vibrational results.

Mode	Frequency, Hz	Mode Shape Type
1	61.39	Bending
2	65.83	Bending
3	73.40	Bending
4	88.69	Bending

Table 3.1 Three-dimensional vibrational analysis frequencies.
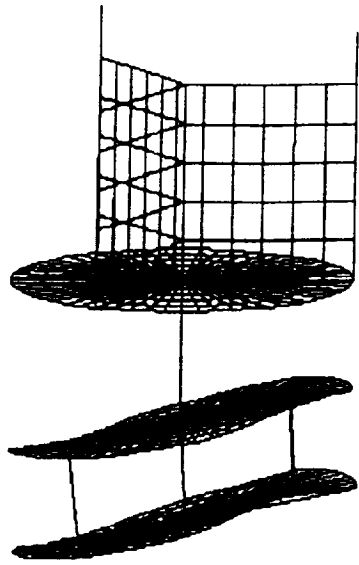
Figure 3.3 Mode shape 1: 61.39 Hz.
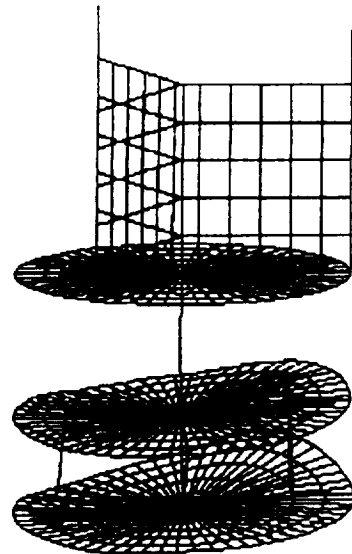
Figure 3.4 Mode shape 2: 65.83 Hz.

11
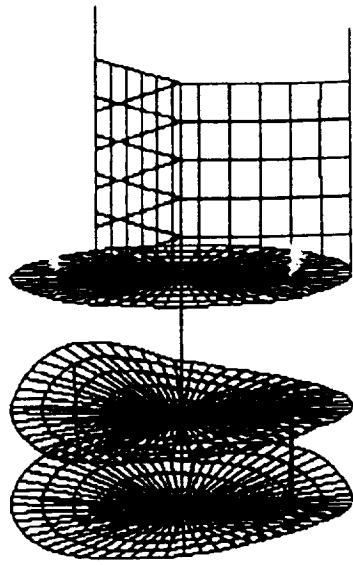
Figure 3.5 Mode shape 3: 73.40 Hz.
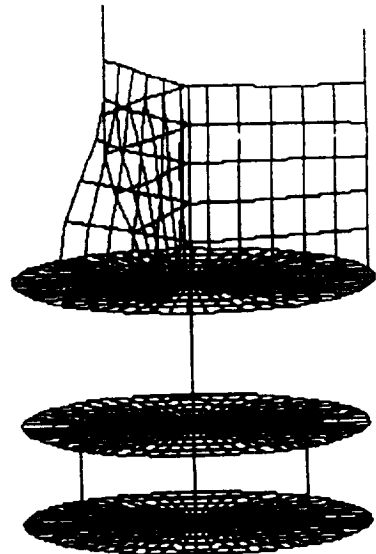
Figure 3.6 Mode shape 4: 80.69 Hz.

4.0. STRUCTURAL ANALYSIS

4.1. ANALYSIS OVERVIEW

The stress analysis for GASCan II was carried out using the IMAGES-3D [1] static analysis capability. Three inertial load cases, specified in NASA's safety manual [2], are applied to the finite element model of the integrated support structure. The maximum Von Mises stress values for each component were used to compute the corresponding margins of safety. In order to verify structural integrity of the support structure, positive margins of safety for each component must be maintained for all load cases. A fail safe analysis is not required since the support structure and all of the experiments are contained by the GASCan superstructure. Failure of any one particular component would not pose a threat to the safety of the shuttle or its crew.

4.2. THREE-DIMENSIONAL STRESS ANALYSIS

4.2.1. Finite Element Model

The finite element model of the support structure in Section 3.2.1 was modified to correctly incorporate the weights and stiffness of the experiments and the battery box. Appendix E details the reasons and methodologies of these modifications. For the analysis, the model is broken into ten components whose names appear in Table 4.1. Otherwise the model and restraints remain identical.

13
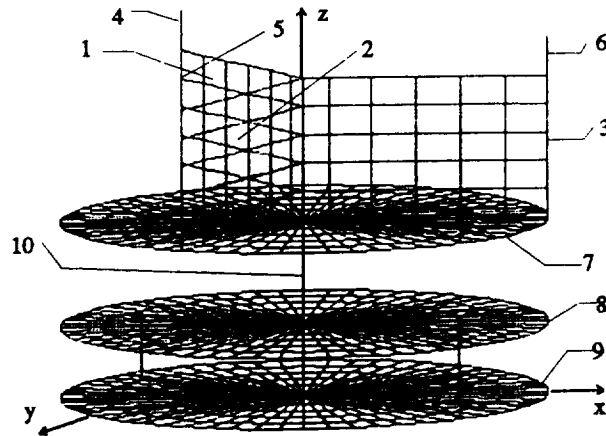
Figure 4.1 Key Components of ISS.

Inertial loadings were applied to the ISS using the inertial body forces option of the IMAGES-3D static analysis capability to carry out the stress analysis. To satisfy NASA safety requirements [2], three separate inertial load cases were employed along each Cartesian coordinate axis. The specific values of limit, yield, and ultimate load cases are stated in Table 4.1. These loadings represent the various accelerations the ISS will encounter while in flight, specifically, launch and landing. To avoid strength verification testing, higher factors of safety were required. "The requirement for strength verification testing can possibly be waived through the use of an increased factor-of-safety (F.S.). This approach would require a positive margin-of-safety for a F.S. greater than or equal to 2.0" [4].

Load Case	x-direction, g's	y-direction, g's	z-direction, g's
Limit	+/- 10.0	+/- 10.0	+/- 10.0
Yield F.S. = 1.5	+/- 15.0	+/- 15.0	+/- 15.0
Ultimate F.S. = 2.0	+/- 20.0	+/- 20.0	+/- 20.0

Table 4.1 Acceleration load cases and factors of safety (F.S.) [10].

4.2.3. Margins of Safety Calculations

The margin of safety (M.S.) is the "ratio of excess strength of a material to the required strength" [4]. The factor is calculated by:

$$M.S = (\sigma_{allowable} / \sigma_{applied}) * F.S$$

where $\sigma_{applied}$ is the von Mises stress obtained from IMAGES-3D and $\sigma_{allowable}$ is either the yield or the ultimate stress of the material. For aluminum 6061-T6, σ_{yield} used for the limit and yield load cases is 36 ksi, and $\sigma_{ultimate}$ for the ultimate load case is 42 ksi [5]. Each component of the support structure must maintain a positive M.S. in every load case to confirm structural integrity.

4.3. STRESS ANALYSIS RESULTS

The von Mises stress contour plots in psi for each load case are shown in Figures 4.2 through 4.4. The contour plots represent the stresses found throughout GASCan II. The highest

15

stress values for each of the ISS components are determined using the maximum nodal stresses found in the IMAGES-3D static analysis output file (ISS3DS.3OU). The maximum nodal stress values are used to cal ulate the margins of safety for all components and for each load case as shown in Table 4.2.

The smallest margin of safety calculated was 2.59 in the ultimate load case. The stress locations are quantitatively and qualitatively consistent with results obtained in the 1992-1993 report. The positive margins of safety verify the structural integrity of the ISS.

To support the reliability of the model, the loads of load case two were applied to the model as separate load cases. This procedure allowed a qualitative analysis which ensured the structure was reacting in a proper manner when all three loads were applied simultaneously. The analysis provided stresses and deflections which were approximately symmetric, agreeing with physical expectations.

The stresses in the support legs returned by IMAGES-3D were also compared to the reaction forces on the legs calculated by hand. The hand analysis did not include the lateral bumpers in the analysis because it is assumed to be a rigid body. However, this comparison qualitatively shows that the finite element model behaves as expected.

As in the vibrational analysis, the stiffness of the lateral bumpers have very recently been updated, along with minor changes to the RFF platform configuration, will require that the FEM structural analysis of the ISS be completed next month.

Key Figure 4.1	Component	M.S. Limit	M.S. Yield	M.S. Ultimate
1	Tri-wall	31.43	8.32	5.45
2	Tri-wall	17.14	8.06	5.28
3	Tri-wall	36.83	16.81	11.04
4	Leg	162.64	72.09	47.30
5	Leg	254.68	113.63	74.57
6	Leg	119.16	53.39	35.04
7	Mid-plate	32.73	15.00	9.84
8	RFF top-plate	7.98	4.01	2.62
9	RFF bot-plate	**7.88**	**3.97**	**2.59**
10	Center Shaft	145.93	64.28	42.83

Table 4.2 Margins of Safety (M.S.) for each load case.

IMAGES-3D
VER. 2.0

0.000
5.807E+2
1.161E+3
1.742E+3
2.322E+3
2.903E+3

Z
Y
X

Load Case
1

Surf: Top

Stress Contour Plot
Von Mises

Figure 4.2 Stress contour plot (psi) limit load case.

18

IMAGES-3D
VER. 2.0

0.000
8.705E+2
1.741E+3
2.611E+3
3.482E+3
4.352E+3

Z

Y

X
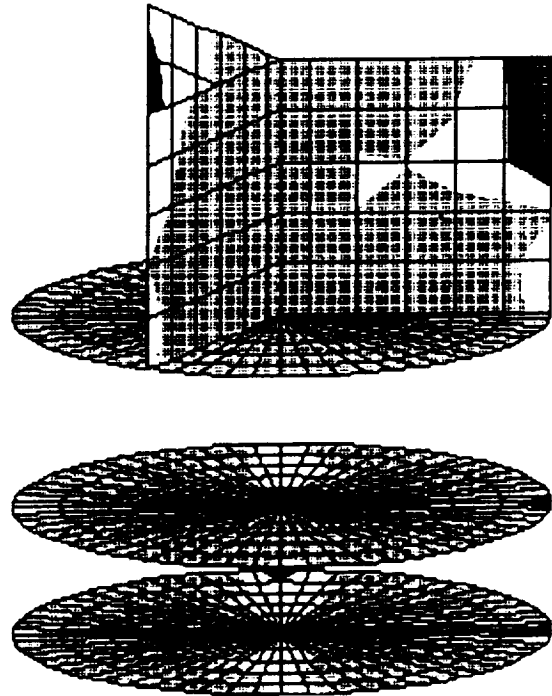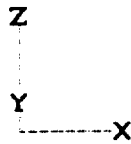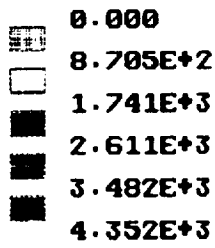
Load Case
2

Surf : Top

Stress Contour Plot

Von Mises

Figure 4.3 Stress contour plot (psi) yield load case.

IMAGES-3D
VER. 2.0

0.000
1.160E+3
2.321E+3
3.482E+3
4.642E+3
5.803E+3

Z
Y
X
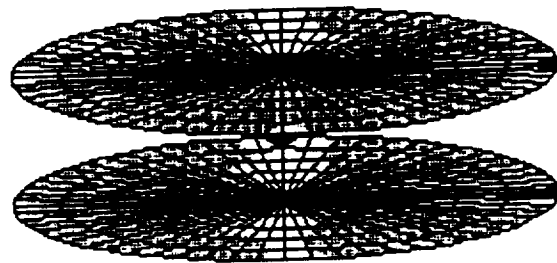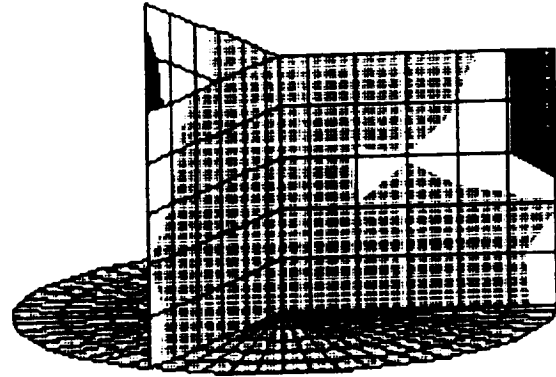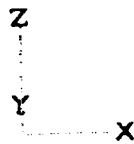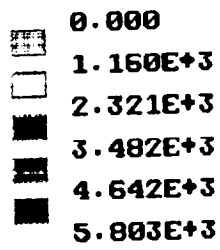
Load Case
3

Stress Contour Plot
Surf: Top   Von Mises

Figure 4.4 Stress contour plot (psi) ultimate load case.

20

5.0. STRUCTURAL ANALYSIS OF CONNECTIONS

This chapter analyzes all the bolted connections in the Integrated Support Structure. The first set of joints examined were the bolted connections between the ISS mounting brackets, the GASCan lid and the ISS tri-walls. The next set of joints examined were the bolted connections of the experiment mounting brackets and the experiments to the tri-walls. Then the welded joints between the tri-wall flanges and the center shaft were scrutinized. Finally the center shaft pin connections were analyzed.

5.1. ANALYSIS METHODOLOGY

5.1.1. Joints and Connections

Each structure mounting bracket is bolted to the GASCan lid with three 3/8"-16 UNC quarter hardened 300 series stainless steel bolts and to the tri-wall flanges with three 1/2"-13 UNC stainless steel bolts.

Each MGI canister is fastened to the tri-walls by means of two connectors designed by the 1993-94 Payload Integration team. Figures 5.1 and 5.2 illustrate the MGI connector and the configuration of the canisters on the flanges, respectively.

The canisters are mounted back to back on each side of the flange with four 1/4"-20 UNC quarter hardened 300 series stainless steel bolts holding both canisters in place.

The boxes containing the IPPE receiver, electrometer, and CPU are fastened to flange C of the tri-wall with four 8-32 UNC quarter hardened 300 series stainless steel bolts per box. Since the CPU board for the MGI experiment is mounted on the opposite side of flange C, the connection will make use of PEM nuts, meaning the nuts corresponding to the IPPE bolts will

21
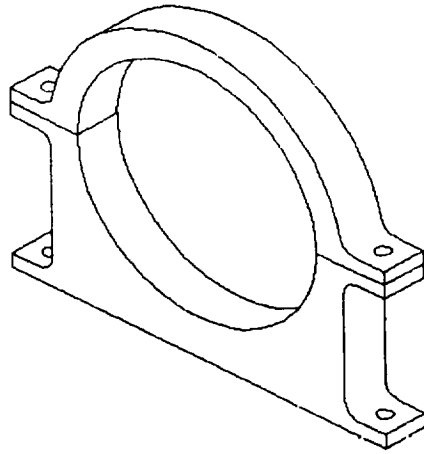
Figure 5.1 MGI mounting bracket.

MGI
connectors

2 1/4″ bolts
per connector
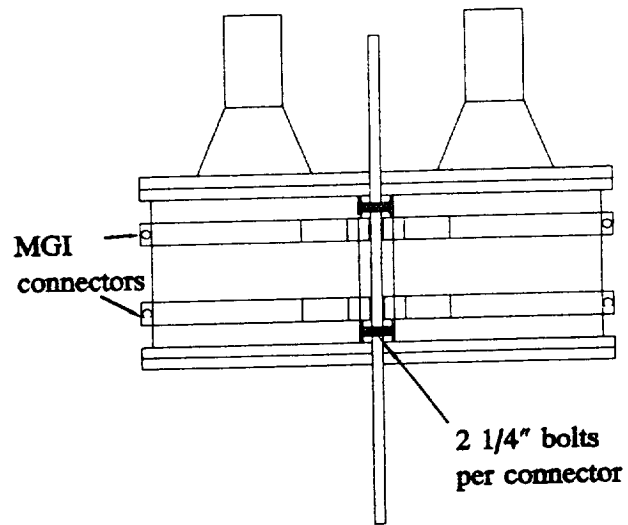
Figure 5.2 Mounting of MGI canisters.

be permanently attached to the flange, behind the MGI CPU.

This will allow the IPPE boxes to be removed without disturbing the MGI CPU. It is recommended for the 1994-95 Payload Integration team that the nuts be welded to the aluminum flange if this is possible.
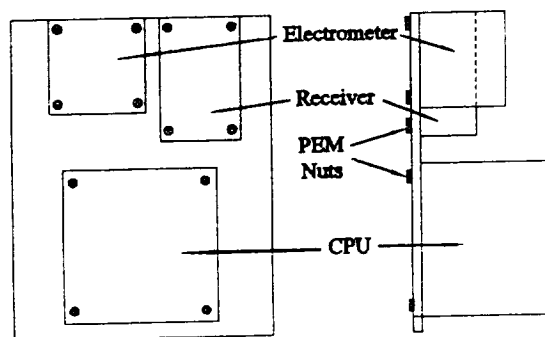
Figure 5.3 IPPE connection.

The welded joints between the tri-wall flanges and the ISS center shaft are continuous for the eleven inch tall double-sided welds approximately 1/4" thick as shown in Figure 5.3.
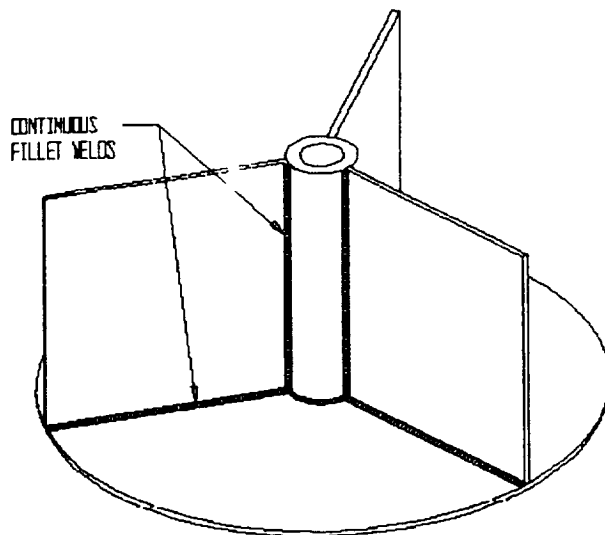
Figure 5.4 Weld configuration for tri-walls.

The center shaft connection is accomplished by fitting the RFF center shaft into the ISS center shaft as shown in Figure 5.5. The connection between the shafts is secured with two 1/4" stainless steel pins located above the midplate.
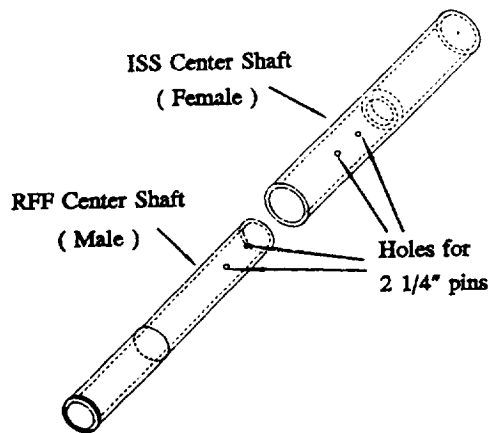
Figure 5.5 Center shaft connection.

24

5.1.2. Analysis Steps

Analysis of the fasteners used in the ISS was conducted by hand, using rigid body models for the structure and the experiments, along with procedures outlined in the NASA Systems Engineering Bolted Joint Handbook [9]. The analysis steps are as follows:

1. Determine forces on each fastener for the load cases given in Table 5.1, assuming static equilibrium.

2. Determine pre-load requirements for each joint (Steps 1, 2 in Appendix H).

3. Determine margins of safety for each fastener (Step 3 in Appendix H).

4. Conduct a failsafe analysis by removing the most severely stressed fastener in the joint and repeating Steps 1 - 3.

5. Determine torque specifications for each joint (Step 4 in Appendix H).

This analysis procedure is detailed for each joint in Appendix F.

5.2. ANALYSIS SUMMARY

5.2.1. Fastener Specifications

Table 5.1. lists margins of safety for three 3/8-16 UNC 300 series quarter hardened stainless steel bolts fastening each structure mounting bracket to the GASCan lid. All of the bolts on each bracket carry the same loads and have the same margin of safety. Calculations supporting these values are included in Appendix I.

	Margins of Safety		Failsafe Margins of Safety	
Flange	Yield	Ultimate	Yield	Ultimate
A	2.50	4.58	1.49	2.76
B	1.45	2.69	0.63	1.13
C	2.26	4.07	1.35	2.43

Table 5.1 Margins of safety for bracket to lid connection.

Margins of safety for 1/2"-13 UNC 300 series quarter hardened stainless steel bolts fastening the structure mounting brackets to the tri-wall flanges are shown in Table 5.2. The lowest margin of safety for each bracket is in bold type. Calculations supporting these values are included in Appendix I.

	Margins of Safety		Failsafe Margins of Safety	
Bolt	Yield	Ultimate	Yield	Ultimate
A-1	**1.72**	**4.28**	**0.91**	**1.70**
A-2	2.23	4.60	1.20	2.20
A-3	1.72	4.28	--	--
B-1	**1.87**	**3.60**	1.39	2.55
B-2	1.93	3.76	1.44	2.68
B-3	1.87	3.60	--	--
C-1	**1.40**	**2.59**	0.52	1.08
C-2	2.15	4.34	0.80	1.52
C-3	1.40	2.59	--	--

Table 5.2 Margins of safety for bracket to tri-wall connection.

Margins of safety for four 1/4"-20 UNC 300 series quarter hardened stainless steel bolts fastening both MGI canisters to flanges A and B are shown in Table 5.3 with the lowest margins of safety in bold type. Calculations supporting these values are included in Appendix F.

Bolt	Margins of Safety		Failsafe Margins of Safety	
	Yield	Ultimate	Yield	Ultimate
A-1	4.68	8.24	**3.68**	**6.16**
A-2	5.05	8.96	4.84	8.10
A-3	**4.20**	**7.35**	--	--
A-4	4.51	7.94	3.76	6.29
B-1	4.55	7.96	**3.51**	**5.87**
B-2	5.04	8.86	4.96	8.30
B-3	**4.09**	7.12	--	--
B-4	4.51	7.88	3.61	6.04

Table 5.3 Margins of safety for MGI canister connection to tri-walls.

Table 5.4 lists margins of safety for the four 8-32 UNC quarter hardened stainless steel bolts fastening each of the IPPE boxes to flange C. The lowest margin of safety for each component in bold type. Calculations supporting these values are included in Appendix F.

27

Margins of Safety					
	Receiver		Electrometer		CPU	
Bolt	Yield	U.timate	Yield	Ultimate	Yield	Ultimate
1	21.4	18.9	28.5	25.7	13.5	11.7
2	23.3	20.8	29.8	27.1	14.6	12.8
3	17.6	15.1	23.7	20.8	9.9	8.25
4	18.8	16.3	24.7	21.7	10.5	8.85

Table 5.4 Margins of safety for IPPE connection to tri-wall.

Joint	Pre-load (lb$_f$)	Torque (in-lb)
Brackets to GASCan lid	1672	125
Brackets to tri-wall	3256	326
MGI cans to tri-wall	300	15

Table 5.5 Pre-load and torque specifications.

The torque and pre-load values listed in Table 5.5. can be obtained by hand tightening the fasteners, without specific measurements. If a turn of the wrench method were used, the measured turn would be four degrees past a snug tight condition. An increment this small is not practical.

5.2.2. Weld Margins of Safety

Appendix G details the analysis of the welded joints between the tri-walls and ISS center shaft. The analysis was performed using values from the IMAGES 3D stress results in the

elements along the center shaft. Fracture analysis on the welds is not necessary since the aluminum 6061-T6 alloy used for the structure has low susceptibility to stress corrosion cracking [6], and the welded joint is classified by NASA as a contained joint [7]. Margins of safety for the most severely stressed weld on each flange are given in Table 5.6.

Weld	M.S. Yield	M.S. Ultimate
A-1	1.515	1.200
B-1	1.941	1.573
C-1	1.298	1.011

Table 5.6 Weld margins of safety.

5.2.3. Center Shaft Connection

The RFF and ISS shafts are connected by two 1/4" 300 series stainless steel pins. The most critically stressed pin has a margin of safety of 5.61 under yield loading conditions and 4.83 under ultimate loading conditions. The analysis of the center shaft joint is detailed in Appendix F.

6.0. BATTERY BOX

One of the main objectives for the 1993 -1994 group was to finalize the design of the container which was to house the batteries for the GASCan II experiments. There were many battery box issues that the team had to consider this year that led to the redesign of the 1992-1993 team's battery box.

6.1. DESIGN

6.1.1. Constraints

Certain specifications had to be followed in order to complete the design of the battery box. These constraints were determined by NASA [2], the battery manufacturer GATES [13], and by the Payload Integration team. The constraints are as follows:

1) The batteries to be used are Gates Sealed-Lead J and X cell batteries.

2) Since the J cell batteries produce significant amounts of hydrogen and oxygen, they must be housed in a container which is: a) sealed, b) corrosion-proof, and c) vented.

3) The battery box must be vented through a) the upper end plate, and b) two 15 psi differential pressure relief valves.

4) The J-cell batteries should be stored in a metal container because hydrogen can permeate a plastic container at a rapid rate.

5) The batteries must supply adequate power to the experiments.

6) Each battery has a volume of:

   J-cell: 15.775 in^3

X-cell: 7.471 in^3

27 J-cells and 12 X-cells are needed to fulfill the power requirement.

7)   The allotted space for the battery box is:

R_{max} = 9.875 in (Radius of middle plate)

$Height_{max}$ = 6.0 in (Space between middle plate and RFF experiment)

8)   Weight must be a factor due to the overall GASCan weight constraint of 200 lb.

9)   The battery box and its interior must be easily accessible. Once the box is removed from the ISS, the batteries must be accessed within 5 minutes.

10)   The battery box design must facilitate electrical hook-up. After mechanically fastening the battery box to the ISS, the two vent lines and all electrical lines must be connected to the outside of the box within 5 minutes.

11)   The X-Cells, in small quantities, do not need to be vented or pressurized [11], while the J-Cells need to be pressurized and vented in any quantity [2].

12)   Batteries of a certain string must be placed in close proximity to each other to facilitate ease of wiring, and they should be packed tightly to prevent them from falling out.

13)   Faulty batteries must be easily accessible for testing and replacement.

6.1.2. Procedure

The battery box designed by the 1992-1993 team was pressurized, vented, and housed 27 J-cells (2.0 V, 12.5 Ah) and 12 X-cells (2.0 V, 5 Ah), as shown in Figure 6.1. This year's team decision to redesign the battery box arose from several issues. It was found that the necessary electrical and venting connections fit too tightly into the
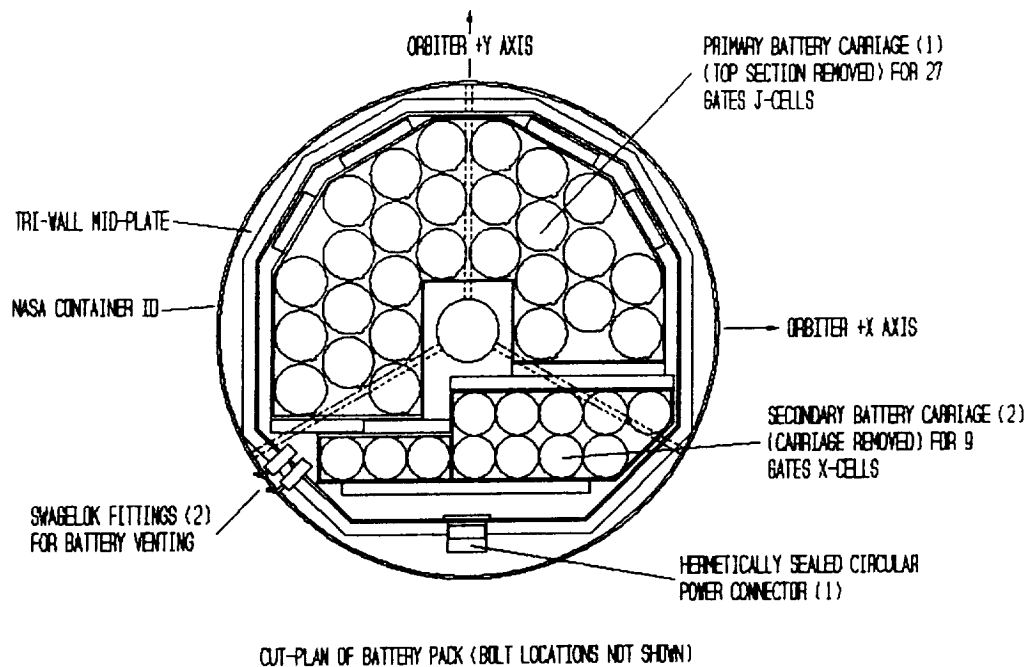
Figure 6.1   1992-93 battery box design.

allotted battery box space. While the X-cells were moved out of the battery box, the J

cells remained since they still must comply with NASA's standards on pressurizing and

venting [2].

Therefore, an initial battery box design used only X-cells so that the pressurization

requirement would be eliminated.   However, in order to meet the necessary power

requirements, a large number of X-cells (63) need to be used.   Although there was a

weight loss associated with this design (14.25%), this idea was not carried through

because: a) the Advanced Space Design faculty members determined that a large number

of X-cells may still be considered an outgassing hazard, and b) a large number of X-cells would not fit in the allotted battery box space.

The 1993-94 team decided to design a new pressurized battery box to house 27 J-cells and to place the remaining 12 X-cells on the tri-wall structure. This simplifies the battery box design because only the batteries that need to pressurized are included in the box. Due to the removal of the X-cells from the box, this allots much more space for the J-cell batteries. The next design step was to split the single cage (as in the previous design) into 3 separate cages. This method involves constructing a cage for the J-cells, similar to those flown in GASCan I. The function of the internal web in the box is to provide a slot-method in which the J-cells could be easily replaced and to insure that the batteries do not fall and short out against each other. Therefore, three cages were designed such that they could each house a string of 9 J-cells, and are connected to the tri-wall mid-plate. Then, the outer battery box can be placed over these cages on the mid-plate. This geometric configuration allows for easy testing and replacement of faulty batteries.

Once the battery box was designed, the team had to determine where and how to place the 12 X-cell batteries up on the tri-wall structure. While this move does simplify the battery box, it also raises a few issues. Due to spacial limitations, the cages were designed (similar to those used in the J-cell case) to house only 3 X-cells each. It is also important to note that these 12 X-cells constitute two necessary battery strings: one string of 3 X-cells that are in series with the main battery loop (the J-cells), and another separate string of 9 X-cells. Therefore, to facilitate easy wiring, at least 3 cages of X-

cells must be in close proximity. Currently, all 4 cages of X-cells will be directly bolted

onto the top of the tri-wall structure.

6.1.3. Structure

As a result of these design changes, the 1993-94 team formulated a new battery
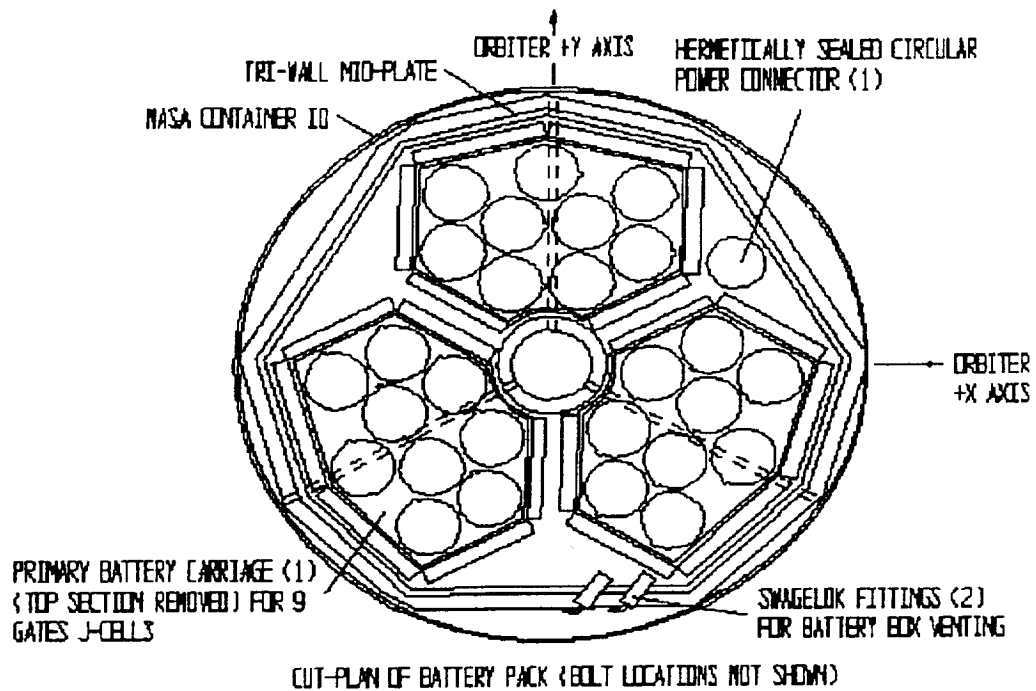
Figure 6.2 Current battery box design.

box layout as shown in Figure 6.2.

6.1.3.1. Enclosure

The battery box assembly is shown in Figure 6.2. The box is a nine-sided shape, constructed of 6061-T6 Aluminum (Appendix B), just under 6" tall, which surrounds the batteries. While the previous design had a .125" wall thickness, the current design must have thicker walls (.25") on the sides where the bumpers will be attached. The enclosure consists of three separate components: the box wall, top plate, and midplate. As in the 1992-93 design, the side-to-bottom seam, as well as all through-wall mounted fittings, are filled with RTV to insure a proper seal. The box is covered by a plate which is

bolted to the sides by 24 0.125" UNC stainless steel (300 series) bolts to compress a 0.0625" thick Viton strip used as a gasket. The whole box is secured to the middle plate with 24 0.1875" UNC stainless steel (300 series) bolts (there are 4 bolts on each of the three longer sides, and 2 bolts on each of the six shorter sides). The battery box is painted with epoxy resign for additional corrosion control in the interior.

Two 15 psi parallel pressure relief valves run from the battery box side, along the canister wall, and into a valve which is mounted on the NASA Experiment Mounting Plate. The plumbing is an assembly of elbows and pipes and is attached to the side wall by nylon straps.

6.1.3.2. Interior

Twenty-seven Gates sealed lead acid J-cells will be housed in the battery box. The three webbed cages provide an inner structure that surrounds the cells and provides support for the cells. Each cage has a cut-out in the bottom to allow the terminals of the battery to come through for easier wiring. The top and bottom of the cages have Neoprene inserts to cushion the batteries and to contain any electrolytic acid leaks. The cages will then be secured by bolting them, through their flanges, to the midplate by 12 .1875" UNC stainless steel (300 series) bolts.

6.2. ELECTRICAL INTERFACE

Important battery information, such as battery layout, mechanical and performance specifications, are included in Appendix J. All wiring between the experiments, the batteries and controller is teflon coated, stranded wire. The internal wiring of the

battery box is fed through a multi-pin, hermetically sealed electrical connector (which will be inside the battery box and will go up through the midplate) to a circuit board located on the tri-wall above the battery box.

Each leg of the strings will be connected with a Schottky diode to prevent reverse current flowing into the battery. The Schottky diode was chosen for its turn-on voltage of .3 Volts. A fuse will be placed between every string of batteries and the ground node for circuit protection. The batteries will be recharged through a separate set of wires connected between the battery terminals and free pins on the NASA connector.

7.0. LATERAL SUPPORT BUMPER DESIGN

The Lateral Support Bumper was redesigned from the 1992-93 MQP design, which was based on the lateral support bumper design used in GASCan I.

7.1. DESIGN

7.1.1. Constraints

The lateral support bumper has several requirements it must meet. The Lateral Support Bumper must:

1) Stay tightened under the structural and vibrational loads that it will encounter during flight.

2) Have a magnitude of stiffness that will reduce the natural frequency of the structure under the NASA specifications.

3) Utilize a realistic tightening procedure.

4) Have more than the prerequisite lateral movement so that the bumper will be tight against the surface of the inner diameter of the GASCan.

5) The bumper must fit in the space between the wall of the battery box and the inner diameter of the GASCan.

7.1.2. Procedure

Using the constraints above, the Payload Integration team designed a lateral support bumper based on the bumper design used in GASCan I and the 1992-93 MQP [12]. The design consists of ten separate pieces, the main bumper body, two 1/8 inch steel pins, an internal wedge, a bumper bracket, 3/8 inch bolt, two nylon locking nuts, a flat washer and a lock washer.

7.1.3. Structure

The main piece of the assembly is the bumper body. Two 1/8 inch pins on either side of the bumper slide-pin the bumper to the bumper bracket. The aluminum bumper bracket positions the bumper at the correct orientation. The stainless steel internal wedge is sandwiched between the bumper body and the bumper bracket. A 3/8"-26 UNC stainless steel bolt, with a 300 series stainless steel lock washer and flat washer, is threaded through the threaded hole in the center of the internal wedge. On the opposite side of the internal wedge, countersunk in an oval pocket, are two nuts with nylon locking inserts, so that the bolt can't loosen during the mission. The assembly is shown in Figure 7.1.

It must be stressed that the nylon locking nuts can be tightened only once, since the nylon locking mechanism is ruined when the bolt is loosened; therefore, extras will be needed. Two nylon lock nuts are required for the fail-safe design required by NASA.

A Viton strip is mounted to the outside face of the bumper body between the bumper and the GASCan. Mounting procedures are outlined in Appendix D.
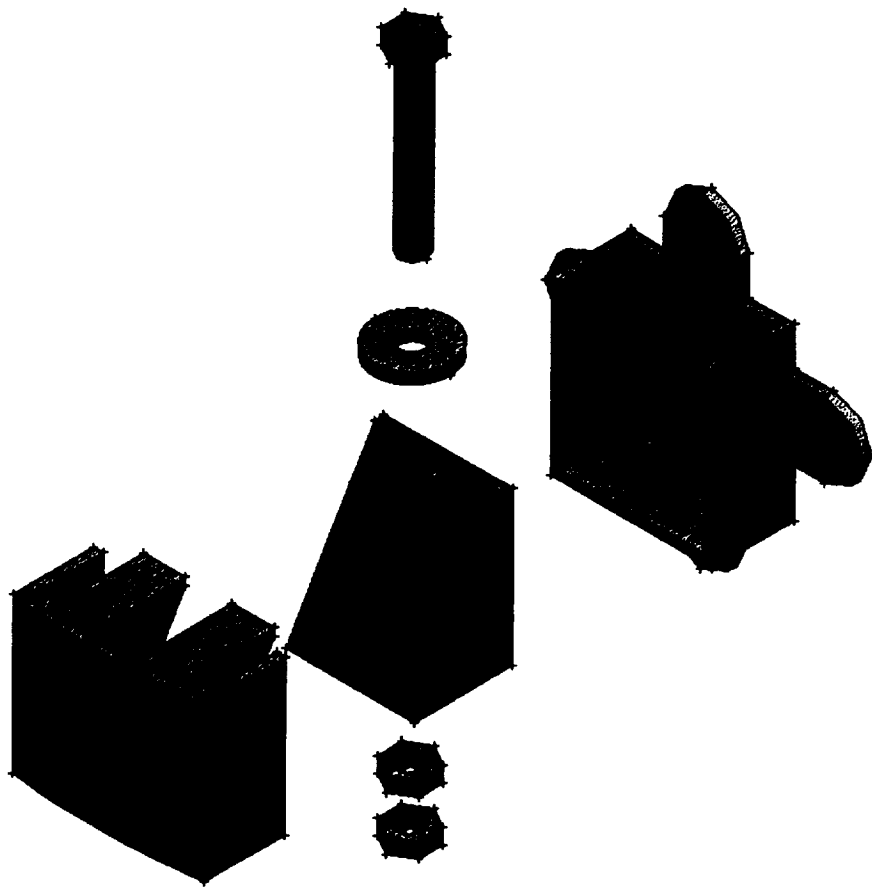
Figure 7.1   Assembly of lateral support bumper.

8.0. IPPE ANTENNA

8.1. ANALYSIS OVERVIEW

Until this project year, no mechanical analysis of the IPPE's antenna receiver had been done. As the IPPE antenna is exterior to the GASCan, it will be carefully examined by the NASA review panel. Should the antenna somehow fail, it could pose a critical risk to crew members or the shuttle mission [2], as opposed to anything contained within the canister. Due to this possibility of this danger, the antenna must meet all requirements of the internal payload, plus the material must satisfy stress corrosion cracking criteria. The IPPE antenna will undergo much the same treatment as the GASCan II and IFS, plus proper material selection [2].

After the MITRE Critical Design Review in '93, it was determined that the largest concern of the previous design was vibrational failure, primarily at the junction between the antenna and the GASCan mounting plate. Under previous recommendations, a vibrational analysis of the IPPE antenna was carried out using the Modal Analysis capability of IMAGES-3D [1]. A three-dimensional finite element model was generated and the first five natural frequencies and corresponding mode shapes were determined using the Subspace Iteration Method. This analysis was conducted to fulfill NASA safety requirements [2] concerning the vibrational integrity of the antenna.

Material options for the antenna itself and the nonconductive support structure at its base were considered and the antenna will be constructed of AMS 5644 stainless steel, with a nonconducting support structure of Delrin or G-10 Fiberglass-Epoxy [11].

41

At this point a stress analysis of the FEM model must be conducted and verified
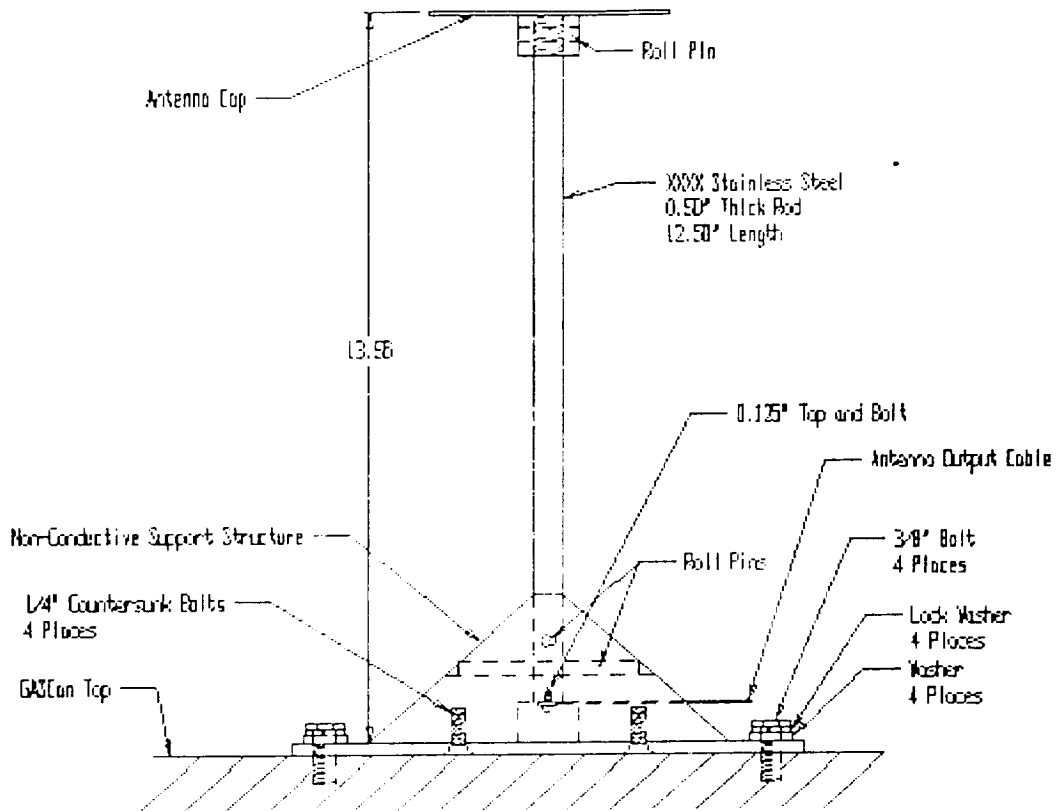
Figure 8.1 IPPE antenna

using hand calculations. A fail-safe analysis of the connecting bolts must also be conducted.

8.2. THREE-DIMENSIONAL VIBRATIONAL ANALYSIS

8.2.1. Finite Element Model

The IPPE Antenna finite element model consists of 85 nodes, 60 four node quadrilateral plate elements, 12 three node triangular

plate elements, and 36 beam elements, creating 693 total degrees of freedom. Appendix M shows the nodal, plate and beam element numbers associated with the antenna top hat and shaft. The material of the support structure is stainless steel AMS 5644, and its mechanical properties can be found in Appendix B. The circular top hat was modeled with quadrilateral and triangular plate elements. Beam elements are used to model the antenna shaft.
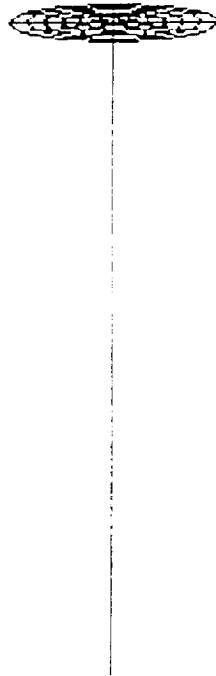
Figure 8.2   Three-dimensional model of
IPPE   antenna.

8.2.2. Model Weight

The total weight of IPPE antenna consists of the top hat, antenna shaft, support base and connections, and is currently estimated at 0.950 lbs. The weights of each component can be found in Appendix M. Beam and plate elements were used to represent the weight of the antenna. The total calculated weight of 0.948 lbs was returned by IMAGES-3D, a difference of 0.2 percent from the actual. The center of gravity returned by IMAGES-3D is stated in Appendix M. The coordinates were verified against those calculated by theoretical methods. The differences between the two centers of gravity is less than 0.08 percent of the length of the antenna along each axis. This calculation is used as a check of the model's reliability.

8.2.3. Boundary Conditions

For a first approximation, the antenna will be assumed to be cantilevered at its base to the GASCan mounting plate. Therefore, the model has to be fully constrained in all six degrees of freedom at the nodes representing this connection as shown in Figure 8.2. This assumption will be disregarded later and the constraints along the six degrees of freedom will be replaced with spring constants that more correctly represent the stiffness of the nonconductive support structure. Rotation in the z-direction has been restrained at the intersection of the beams of the shaft and the plate elements that represent the antenna top hat. This restraint is necessary to avoid a singular solution error occurring when beam and plate elements intersect orthogonally. The beam has a rotational degree of freedom along its length while the plate element has no inplane

rotational degree of freedom. The node where they join must be restrained in the local

z-rotation to suppress a local rigid body rotational motion.

8.2.4. Three-Dimensional Vibrational Analysis Results

The first five natural frequencies and mode shapes for the IPPE antenna are stated

in Table 8.1. The fundamental frequency of 57.44 Hz is greater than the 51 Hz required

by the NASA Simplified Options for STS Payloads [4], thus verifying the vibrational

integrity of the IPPE Antenna.

Mode	Frequency, Hz	Mode Shape Type
1	57.44	Bending (S)*
2	57.44	Bending (S)*
3	402.9	Bending (S)*
4	402.9	Bending (S)*
5	571.9	Bending (TH)*

Table 8.1 Three-dimensional vibrational analysis frequencies
(S)* Bending in the antenna shaft
(TH)* Bending in the antenna top hat

45
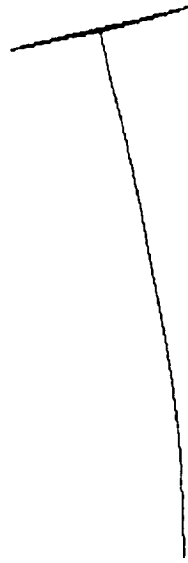
Figure 8.3 Mode shapes 1 and 2:
57.44 Hz.
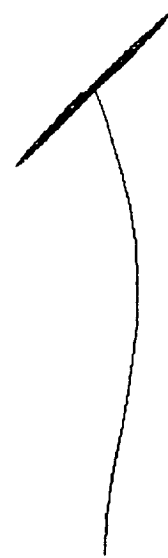
Figure 8.4 Mode shapes 3 and 4:
402.9 Hz.

Figure 8.5 Mode shapes 5 and 6: 571.9 Hz.

Load Case	x-direction, g's	y-direction, g's	z-direction, g's
Limit	+/- 10.0	+/- 10.0	+/- 10.0
Yield F.S. = 1.5	+/- 15.0	+/- 15.0	+/- 15.0
Ultimate F.S. = 2.0	+/- 20.0	+/- 20.0	+/- 20.0

Table 8.2 Acceleration load cases and factors of safeties (F.S.) [10].

8.4.3. Margin of Safety Calculations

The margin of safety (M.S.) are calculated as in section 4.3 for GASCan II by:

$$M.S = (\sigma_{allowable} / \sigma_{applied}) * F.S$$

where $\sigma_{applied}$ is the von Mises stress obtained from IMAGES-3D and $\sigma_{allowable}$ is either the yield or the ultimate stress of the material. For stainless steel AMS 5644, σ_{yield} used for the limit and yield load cases is 130 ksi, and $\sigma_{ultimate}$ for the ultimate load case is 170 ksi [5]. Each component of the support structure must maintain a positive M.S. in every load case to confirm structural integrity.

8.4.4. Three-Dimensional Stress Analysis Results

The highest stress values for the IPPE antenna are determined using the maximum nodal stresses found in the IMAGES-3D static analysis output file (ANTENNA.3OU). The maximum nodal stress values are used to calculate the margins of safety for all components and for each load case as shown in Table 8.2.

The smallest margin of safety calculated was 0.76 in the ultimate load case. The stress locations are quantitatively and qualitatively consistent with hand calculations. The positive margins of safety verify the structural integrity of the antenna.

Key Figure 8.1	Component	M.S. Limit	M.S. Yield	M.S. Ultimate
1	Top Hat	335.7	159.1	155.1
2	Shaft	1.68	0.79	0.76

Table 8.2 Margins of Safety (M.S.) for each load case.

0.000

9.401E+1

1.880E+2

2.820E+2

3.760E+2

4.700E+2

Y

Z——X
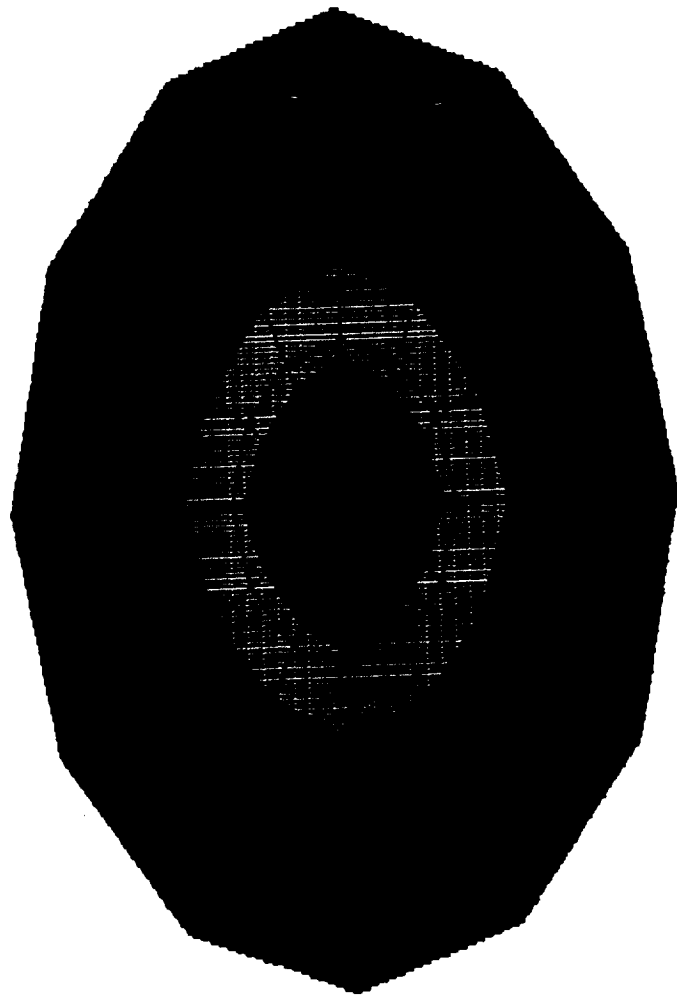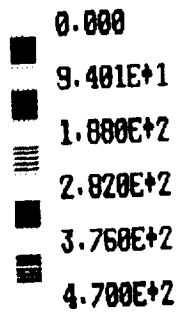
Figure 8.6   Stress contour plot (psi) limit load case of
IPPE top hat.

IMAGES-3D
VER. 2.0

0.000
1.410E+2
2.820E+2
4.230E+2
5.640E+2
7.051E+2

Y

Z———X
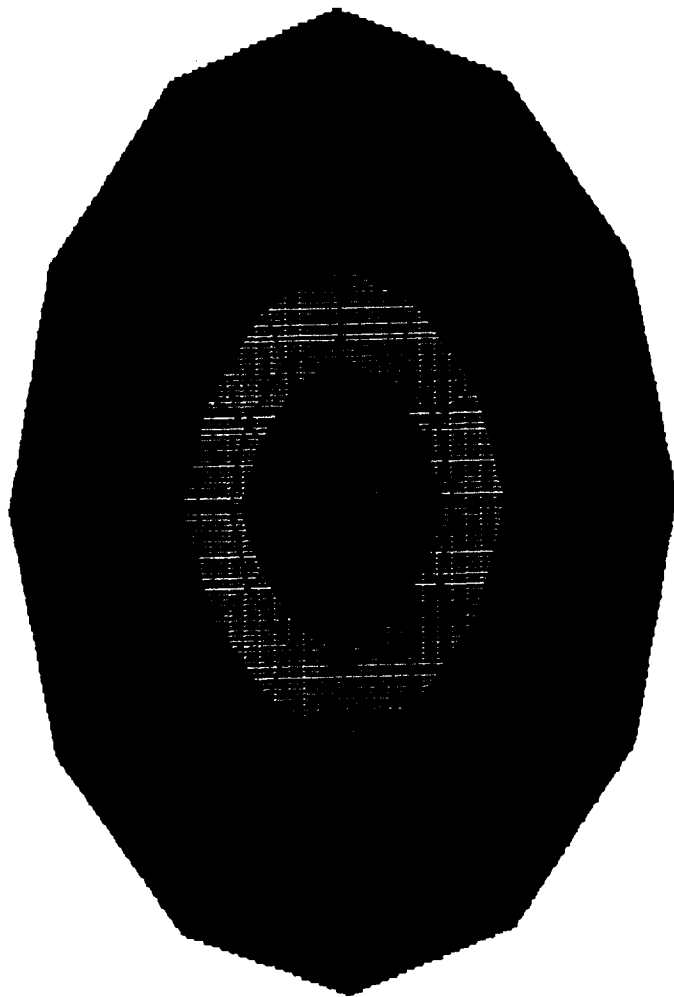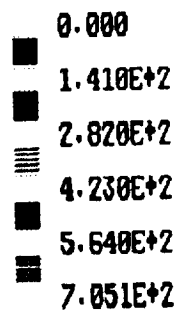
Figure 8.7 Stress contour plot (psi) yield case of IPPE antenna.

52

IMAGES-3D
VER. 2.0

0.000
1.880E+2
3.760E+2
5.640E+2
7.521E+2
9.401E+2

Y
Z———X
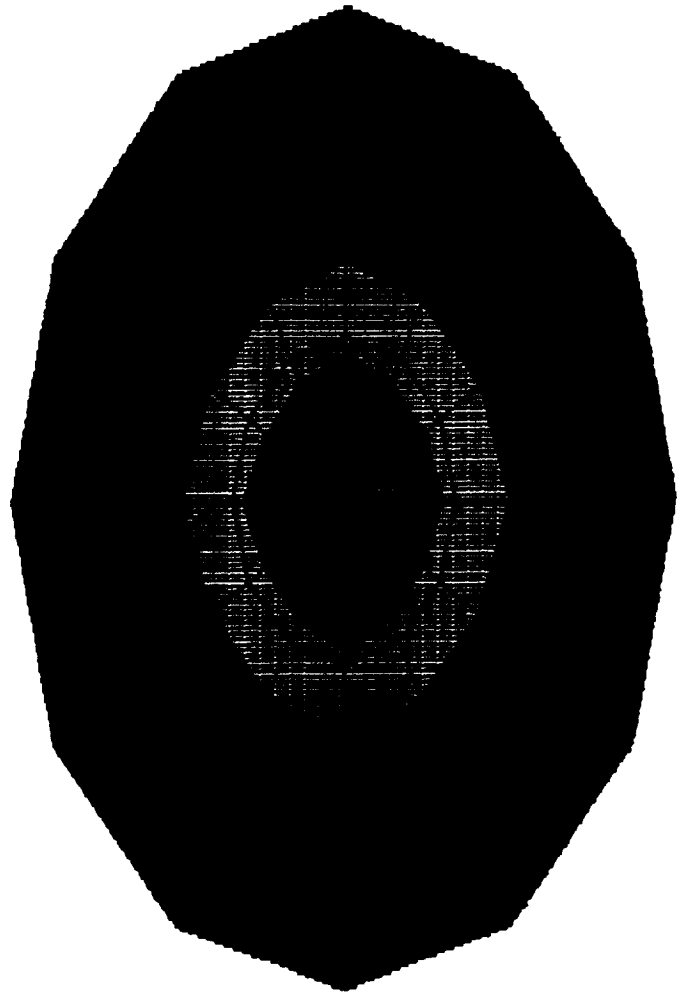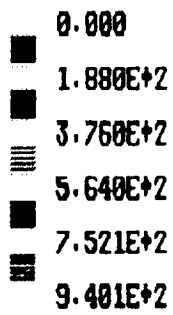
Figure 8.8 Stress contour plot (psi) ultimate case for IPPE antenna.

53

9.0. MICRO-GRAVITY IGNITION BRACKETS

9.1. DESIGN

Another issue for this year's team was the Micro-Gravity Ignition Brackets. In past years, the bracket design was not examined thoroughly. The previous design consisted of a simple, thin, metal band which was strapped around the Micro-Gravity Ignition cylinders. Therefore, a stronger bracket had to be designed.

9.1.1. Constraints

The following design constraints were determined by the Payload Integration team for the brackets:

1) Brackets must be able to support the weight of each Ignition canister.

2) Brackets must attach each cylinder to the tri-wall structure safely.

3) Bracket bolts must be able to resist separation, and satisfy strength and vibrational requirements [2].

9.1.2. Procedure

An initial bracket design was given to the Integration team by the Micro-Gravity Ignition team. Major dimensions, such as the inner diameter, bolt diameter, width, and length, were already established. However, there were some dimensions that needed to be finalized.

Given the .25" diameter of the bolts, it was necessary to determine the thickness of the material being held together by the bolts that would withstand static and fatigue loadings. This is important since the cylinder-bracket assembly cannot separate from the

tri-wall structure during the space shuttle flight. In this case, both static (due to cylinder weight) and fatigue (due to vibration) loadings need to be accounted for. This analysis process was carried out in accordance with Shigley's [8] textbook.

In order to ensure safety during the space shuttle flight, a stress analysis was carried out for the brackets and bolts. All analyses yielded relatively small stresses due to a combination of low weight and the high strength of the bracket and bolts. The analysis methodology for the bracket connections and a sample calculation is presented in Appendix N. This analysis ensures that the bolts will not fail. In order to ensure proper safety, a simple stress analysis was conducted for the bracket. If these safety requirements are met, the bolts and brackets will not fail during the space shuttle flight.

Another design modification was then made to the original design. In order to hold the brackets securely against the cylinders, it was decided to add an O-ring to the assembly. Therefore, this modification will keep the bracket "snug" against the cylinder, eliminate movement, and act as a spacer.

9.1.3. Structure

The finalized Micro-Gravity Ignition Bracket design is shown in Figure 9.1. As mentioned earlier, these brackets will attach the Micro-Gravity Ignition cylinders to the tri-wall structure. Eight brackets will be required and two brackets will be used for each cylinder. The brackets will be made of 6061-T6 Aluminum [Appendix B], while the bolts will be 1/4" UNC 300 series stainless steel. Two bolts will attach the brackets to the tri-wall and the other two bolts will tighten the bracket around the cylinder.
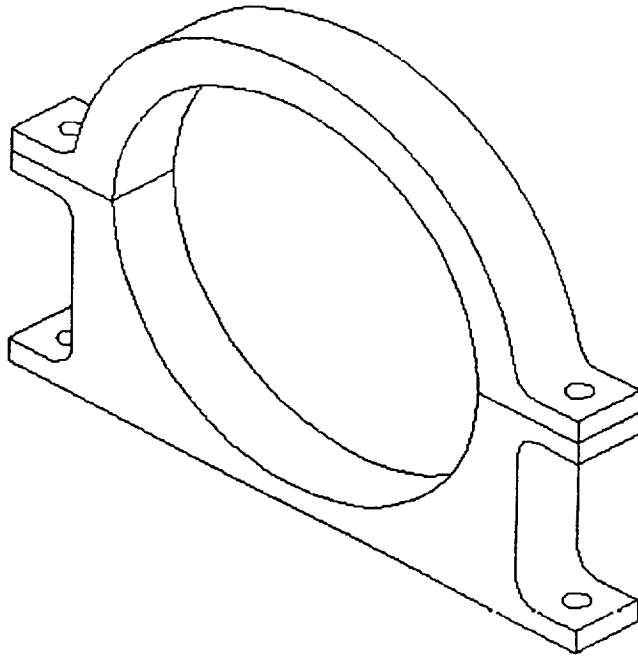
Figure 9.1 Micro-gravity ignition bracket.

10.0. POWER SUPPLY AND ELECTRICAL CONNECTIONS

The purpose of this project is to provide power to the three experimental packages that comprise GASCan II. This report contains information on the battery configuration, the wiring layout, external charging features, and the external power connection feature.

Power for GASCan II will be supplied from a central battery box which consists of twenty-seven Gates J-Cells (2.0V 12.5Ah) and twelve Gates X-Cells (2.0V 5Ah). The maximum total power supplied from these batteries is 795Wh. At the time of launch, the derated power is 373Wh; this derated value assumes that the batteries once charged remain unused for 90 days. Table 10.1 shows the power consumed by each experiment, while Table 10.2 provides information on the power available. From the battery box, the power is routed to NASA power-control relays, then to the power distribution box, and finally to the experiments.

10.1. BATTERY BOX

The following paragraphs describe how the various supply voltage required by the experiments is provided:

EXPERIMENT	VOLTAGE (V)	CURRENT (A)	DURATION	POWER (Wh)
MICRO-G	+24	8	100sec	5.33
	+18	0.040	120sec	0.024
	+ 9	2	120sec	0.6
	-18	0.040	120sec	0.024
IPPE	+18	0.230	48hr	198.7
	+18	0.060	32hr	34.56
	+12	0.011	48hr	6.34
	+12	0.0175	48hr	10.08
	+12	0.014	32hr	5.38
	-18	0.005	32hr	2.88
	-12	0.014	48hr	8.06
	-12	0.014	32hr	5.38
RFF	+18	0.6	7hr	75.6
	+12	0.0571	7hr	4.8
	+ 5	0.0571	7hr	2
	-12	0.0143	7hr	1.2

Table 10.1 Power consumption table.

TOTAL POWER:

MGI = 6.0Wh
IPPE = 271.4Wh
RFF = 83.6Wh

+ _____

361.0 Wh

STRING	# OF STRINGS	# OF CELLS ON EACH STRING	CELL VOLTAGE	CURRENT CAPACITY	POWER
A	1	9	2.0V	12.5Ah	225Wh
B	2	9	2.0V	12.5Ah	450Wh
C	1	3	2.0V	5Ah	30Wh
D	1	9	2.0V	5Ah	90Wh

Table 10.2 Power available.

TOTAL POWER: 795 Wh
DERATED POWER: 373 Wh

• Nine J-Cells are connected in series to supply +18V (String A). This string is used only by the Rotational Fluid Flow experiment to run its platform drive motor and fluid circulation pump. Separating this power supply reduces the chance of polluting other power supply circuits with conducted noise generated by the DC motors.

• Eighteen J-Cells are connected in two parallel strings with nine cells on each string (String B1 and String B2). Diodes are placed in series with each string leg to prevent reverse current from flowing into the battery. The combination of these two string supplies the +18V (String B).

• Three X-Cells are connected in series with string B to provide +24V (String C).

• Nine X-Cells are connected in series to supply -18V (String D). Figure 1, Appendix P shows the details of the wiring inside the battery box. The diodes used to prevent reverse current flow are Schottky diodes. This type of diode has a turn-on voltage of only 0.3V. Two fuses are located on each string. This is a precaution of their being

59

damaged by the heavy vibration encountered when the space shuttle is launched.

10.2. NASA RELAYS AND CONNECTOR

From the battery box, the power is routed to the NASA Connector. During the actual mission, this connector will be coupled with relays A, B, and C of the NASA Gas Control Decoder (GCD). Relay A controls Payload Power Contactor which contains two contacts. These contacts are used to control String A and String B of the GASCan II power supply. GCD B is connected to String C, and GCD C is connected to String D as shown in Figure 2, Appendix O.

10.3. EXTERNAL CHARGING AND EXTERNAL POWER CONNECTIONS

An external charging option is also incorporated. The battery power supply can be charged from outside of the canister through use of free pins on the NASA Connector. Special attention is necessary for String B1 and B2. In particular, additional wiring to bypass the reverse-current diodes is needed to perform the task.

There are also pins on the NASA connector dedicated for inter connection of external power. This feature is used during the ground diagnostic process. When diagnostic procedures are performed, power can be supplied externally so that the energy stored in the battery supply is not depleted.
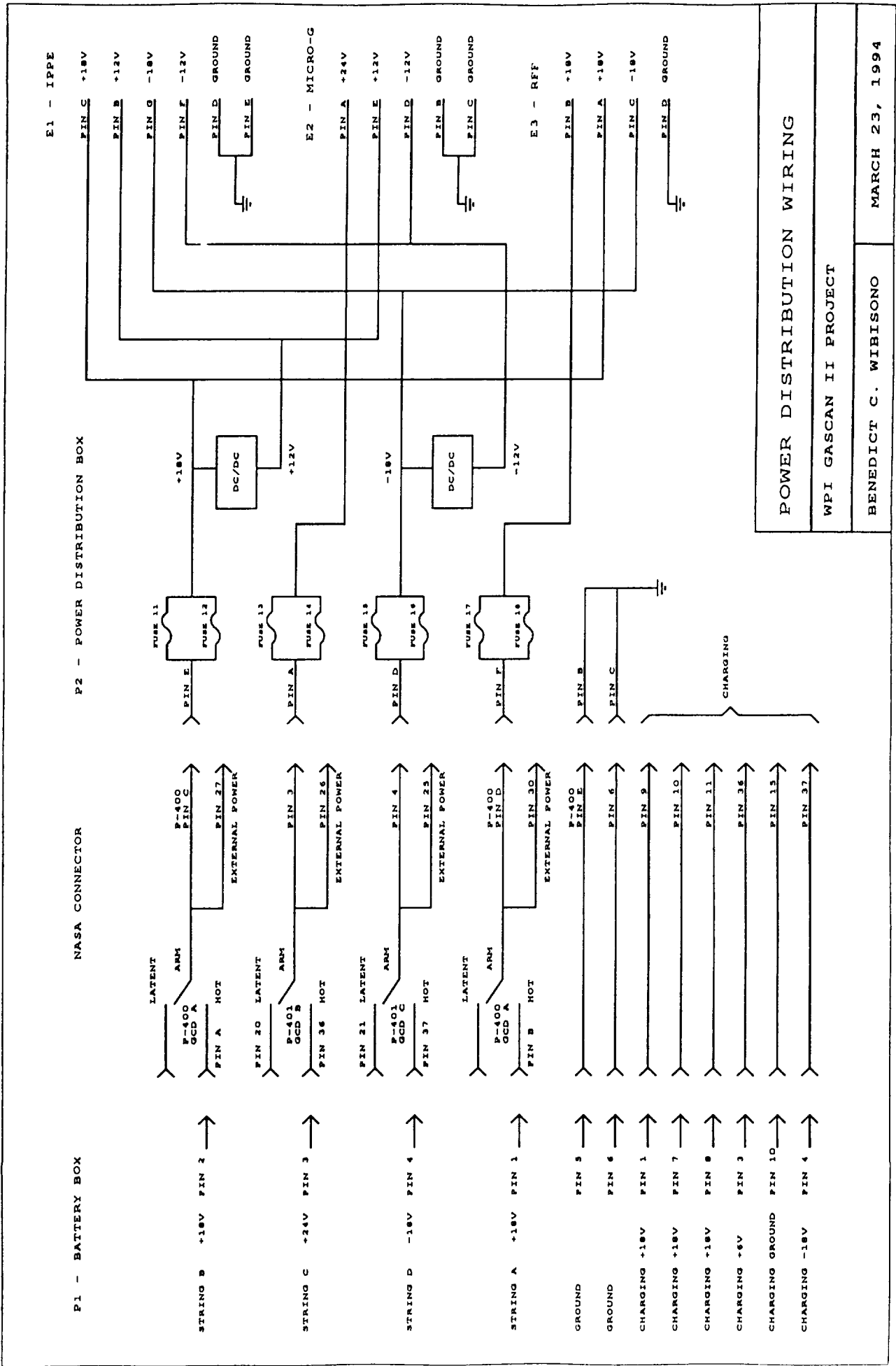
POWER DISTRIBUTION WIRING

WPI GASCAN II PROJECT

BENEDICT C. WIBISONO   MARCH 23, 1994

E1 - IPPE

- PIN C   +18V
- PIN B   +12V
- PIN G   -18V
- PIN F   -12V
- PIN D   GROUND
- PIN E   GROUND

E2 - MICRO-G

- PIN A   +24V
- PIN E   +12V
- PIN D   -12V
- PIN B   GROUND
- PIN C   GROUND

E3 - RFF

- PIN B   +18V
- PIN A   +18V
- PIN C   -18V
- PIN D   GROUND

P2 - POWER DISTRIBUTION BOX

+18V   DC/DC   +12V
-18V   DC/DC   -12V

FUSE 11   FUSE 12   PIN E
FUSE 13   FUSE 14   PIN A
FUSE 15   FUSE 16   PIN D
FUSE 17   FUSE 18   PIN F

PIN B
PIN C

CHARGING

P1 - BATTERY BOX

NASA CONNECTOR

LATENT   ARM   HOT
P-400 GCD A   PIN A
P-400 PIN C   PIN 27
EXTERNAL POWER

PIN 20   LATENT   ARM   HOT
P-401 GCD B   PIN 36
PIN 3
PIN 26
EXTERNAL POWER

PIN 21   LATENT   ARM   HOT
P-401 GCD C   PIN 37
PIN 4
PIN 25
EXTERNAL POWER

LATENT   ARM   HOT
P-400 GCD A   PIN B
P-400 PIN D   PIN 30
EXTERNAL POWER

P-400 PIN E
PIN 6
PIN 9
PIN 10
PIN 11
PIN 36
PIN 15
PIN 37

STRING B   +18V   PIN 2
STRING C   +24V   PIN 3
STRING D   -18V   PIN 4
STRING A   +18V   PIN 1
GROUND   PIN 5
GROUND   PIN 6
CHARGING +18V   PIN 1
CHARGING +18V   PIN 7
CHARGING -18V   PIN 8
CHARGING +6V   PIN 3
CHARGING GROUND   PIN 10
CHARGING -18V   PIN 4

PIN 4 −18V STRING D CHARGING

X4 X5 X6 X7 X8 X9 X10 X11 X12

FUSE 9 FUSE 10

PIN 2 +18V STRING B

PIN 3 +24V STRING C CHARGING

PIN 10 CHARGING GROUND

PIN 5 GROUND

PIN 6 GROUND

X1 X2 X3

FUSE 7 FUSE 8

+18V

D4
D3
PIN 8 STRING B2 CHARGING

J19 J20 J21 J22 J23 J24 J25 J26 J27

FUSE 5 FUSE 6

D2
D1
PIN 7 STRING B1 CHARGING

J10 J11 J12 J13 J14 J15 J16 J17 J18

FUSE 3 FUSE 4

PIN 1 +18V STRING A CHARGING

J1 J2 J3 J4 J5 J6 J7 J8 J9

FUSE 1 FUSE 2

BATTERY CONFIGURATION

WPI GASCAN II PROJECT

BENEDICT C. WIBISONO   MARCH 23, 1994

B

11.0. CONCLUSIONS

The overall design of GASCan II is finalized. All experiments have met their allocated space and weight requirements. All engineering and part drawings are complete and can be found in the appendices, leaving only the actual construction of GASCan II to the 1994-95 team.

GASCan II has met NASA safety requirements for both the vibrational and stress analysis. Finite element analyses results show the ISS fundamental frequency to be greater than that required by NASA [1]. Positive margins of safety were calculated, for the ISS and each experiment connection using both IMAGES-3D and hand calculations, for the limit, yield, and ultimate inertial load cases. Finally, a fail-safe analysis was made by removing the most critical bolt from the analysis of each experiment and support leg, resulting in a positive margin of safety.

12.0. FUTURE WORK

The 1993-94 Integration team recommends that the 1994-95 team address the following:

1. Integrated Support Structure

Components of the ISS and experiments have been manufactured. However, the 1994-95 team will need to finalize placement of connections on first the mock-up, and then the actual structure. Holes will need to be drilled for the MGI cylinder brackets and CPU, IPPE equipment and center shaft pins for RFF platform.

Due to very recent updates in the stiffness of the lateral support bumpers and adjustments to RFF platform configuration, the vibrational and stress FEM models of GASCan II will be rerun in the next month.

2. Battery Box

The finalized design of the battery box needs to be constructed. The team needs to contact the MITRE engineers in order to start construction of the battery cages. Steve Derosier should be consulted on the fabrication of the actual battery box. Special attention should be paid to the structural integrity of the box walls. After the battery box is constructed, the placement of the bolt holes will become apparent. The box will need to be pressurized and vented as stated in Chapter 6, and the power connector will need to be installed.

3. Lateral bumpers

The lateral bumper design is finalized. However, if the natural frequency of the ISS drops lower than the NASA specifications, then the aluminum bumper body will need

to be made out of stainless steel to increase its stiffness. The bumpers will need to be constructed. Six bumpers will be needed in case the GASCan needs to be disassembled at NASA for equipment failure. This is due to the nylon locking nuts that will be permanently attached in the internal wedge.

4. IPPE Antenna

A first vibrational and stress FEM analysis of the IPPE antenna have been completed, both of which meet NASA safety requirements for structural integrity. The simplified cantilever assumption at the base must be replaced with spring elements which more closely represent the actual antenna base. The question of whether to use Delrin or G-10 fiberglass epoxy for the base support must also be answered.

5. Micro-Gravity Ignition Brackets

The MGI bracket design has been finalized. However, the brackets need to constructed. Steve Derosier should be contacted about this.

6. Electrical Interface

Before the electrical design is finalized, some additional consideration should be given to the method used to obtain external power. With the present design, each experimental package currently assumes that it is in the space environment as soon as power is supplied to it. A more appropriate procedure is needed to assure that each experiment is able to distinguish logically between ground diagnostic procedures and space operation.

7. Final Integration

With the finalization of GASCan II due in 1995, it is imperative that the

construction of all components be started early next year. The 1994-95 team will need to ensure all placement of components is finalized through the use of the wooden mock-up. Once the final bolt locations are determined, GASCan II should be constructed. The 1994-95 team will need to communicate with the WPI machine shop in order to ensure successful fabrication of all components.

REFERENCES

1. Celestial Software Inc., *IMAGES-3D*, Version 2.0, 2150 Shattuck Ave, Suite 1200, Berkeley, California, 94704, 1990.

2. National Aeronautics and Space Administration, *Get Away Special Payloads - Safety Manual*, 1986.

3. MITRE/WPI Space Shuttle Program G-408 *GASCan I Safety Data Package*, September 30, 1986.

4. Hamilton, D.A., *Simplified Design Options for STS Payloads*, Lyndon B. Johnson Space Center, Houston, Texas, 1985.

5. "Metallic Materials and Elements for Flight Vehicle Structures," *Military Standardization Handbook*, MIL-HDBK-5C, 1976.

6. *Design Criteria for Controlling Stress Corrosion Cracking*, National Aeronautics and Space Administration, Marshall Space Flight Center, Alabama, November, 1990.

7. *General Fracture Control Plan for Payloads using the Space Transportation System*, National Aeronautics and Space Administration, Langley Research Center, Virginia, November, 1988.

8. Shigley, J. E., *Mechanical Engineering Design*, 5th edition, McGraw Hill: New York, 1989.

9. *Systems Engineering Division Bolted Joint Handbook*, National Aeronautics and Space Administration, Langley Research Center, Virginia, November, 1990.

10. *GAS Experimenter's Guide to the STS safety Review Process and Data Package Preparation*, National Aeronautics and Space Administration, Goddard Space Flight Center, Greenbelt, Maryland, 1993.

11. Mark Peten, National Aeronautics and Space Administration, Goddard Space Flight Center, Greenbelt, Maryland, 1993.

12. Ard, P., Roszkowski, M. and Wall, S., *1993-94 Advanced Space Design Integrated Support Structure Major Qualifying Project*, Mechanical Engineering Department, Worcester Polytechnic Institute, Worcester, Massachusetts, 1994.

13. Gates Energy Products Inc., *Gates' Battery Applications Manual*, Gainesville, Florida 32602.

APPENDIX A

BEAM/PLATE ELEMENT NUMBERS OF ISS COMPONENTS

APPENDIX A

BEAM/PLATE ELEMENT NUMBERS OF ISS COMPONENTS

Key, Figure 6.1	Component	Range of Beam/ Plates
1	Leg	16-20, 115 beams
2	Leg	21-25, 116 beams
3	Leg	25-30, 117 beams
4	Tri-Wall	1081-1110 plates
5	Tri-Wall	1111-1140 plates
6	Tri-Wall	1141-1170 plates
7	Midplate	721-1080 plates
8	RFF Top Plate	361-720 plates
9	RFF Bottom Plate	1-360 plates
10	Center shaft	1-15 beams

APPENDIX B

STRUCTURAL MATERIAL PROPERTIES

APPENDIX B

STRUCTURAL MATERIAL PROPERTIES [5]

ALUMINUM 6061-T6

Density:	0.098 lb/in^3
Young's Modulus:	9.9x10^6 psi
Poisson's Ratio:	0.33
Yield Strength:	36x10^3 psi
Ultimate Tensile Strength:	42x10^3 psi

STAINLESS STEEL AMS 5644

Density:	0.276 lb/in^3
Young's Modulus:	29x10^6 psi
Poisson's Ratio:	0.28
Yield Strength:	140x10^3 psi
Ultimate Tensile Strength:	170x10^3 psi

APPENDIX C

COMPONENT WEIGHTS AND LOCATIONS

APPENDIX C

COMPONENT WEIGHTS AND LOCATIONS

EXPERIMENT WEIGHTS

COMPONENT	NUMBER	WEIGHT (LB)
IPPE CPU	1	4.83
MICRO-G CANS	4	5.9/CAN
RFF PLATFORM AND CENTERPIECE	1	14.0
FLUID CYLINDER	4	5.9
CAMERA	1	1.8
PUMP, MIRROR, AND PIPING	1	1.3
FLUID, WIRING, PLUMBING, (ESTIMATION)	1	15.0
BATTERY BOX	1	64.5
X-CELL CAGES	4	3.0/CAGE
POWER DISTRIBUTION	1	5.0

SUBTOTAL   147.93 LBS

SUPPORT STRUCTURE WEIGHT

COMPONENT	NUMBER	WEIGHT (LB)
TRI-WALL	3	2.6/WALL
MIDPLATE	1	7.385
ISS SHAFT	1	1.2796
RFF SHAFT	1	2.9874
LEGS	3	0.861/LEG
BUMPERS	3	0.75/BUMPER

SUBTOTAL   24.29 LBS
TOTAL   172.22 LBS
MAXIMUM ALLOWABLE 200.0 LBS

3

TABULATED COORDINATES FOR THE CENTER OF MASS
FOR EACH COMPONENT

COMPONENT	WT (lb)	X (in)	Y (in)	Z (in)
IPPE CPU	4.83	-2.156	3.375	19.875
2 MGI CANS ON FLANGE A	11.80	4.313	0	19.875
2 MGI CANS ON FLANGE B	11.80	-2.156	-3.735	19.875
RFF PLATES AND CENTERPIECE	14.0	-.627	-1.613	3.875
RFF FLUID CYLINDER	6.3	0.48	6.32	0.25
RFF CAMERA	1.94	-2.089	-6.0	0.25
RFF PUMP	1.33	2.63	-6.78	0.25
RFF MIRROR	0.73	-5.44	6.53	0.25
RFF BUBBLE SENSOR	0.52	6.25	4.63	0.25
RFF ULTRASONICS	0.52	5.13	5.13	0.25
RFF CPU	2.26	4.91	-0.22	0.25
BATTERY BOX	64.5	0	0	10.375
X-CELL CAGES ON FLANGE A	6.0	2.765	0	22.255
X-CELL CAGES ON FLANGE B	6.0	-1.382	-2.395	22.255
3 TRI-WALLS	7.8	0	0	19.875
MIDPLATE	7.5	0	0	14.375
ISS SHAFT	1.28	0	0	16.813
RFF SHAFT	2.99	0	0	8.75
3 MOUNTING BRACKETS	2.58	0	0	25.75

HAND ANALYSIS CENTER OF MASS $\bar{X}=.196$ $\bar{Y}=-.0168$ $\bar{Z}=13.9$

FEM MODEL CENTER OF MASS $\bar{X}=.386$ $\bar{Y}=-.2415$ $\bar{Z}=13.01$

The hand analysis center of mass was calculated using the following equations.

$$\bar{X} = \frac{\sum (X_i \ W_i)}{\sum W_i}$$

$$\bar{Y} = \frac{\sum (Y_i \ W_i)}{\sum W_i}$$

$$\bar{Z} = \frac{\sum (Z_i \ W_i)}{\sum W_i}$$

Where X_i, Y_i, Z_i, are the respective coordinates of each component, treated as point masses, and W_i is the weight of each component.

5

APPENDIX D

NODAL LOCATIONS OF CONCENTRATED WEIGHTS FOR

VIBRATIONAL ANALYSIS

APPENDIX D

NODAL LOCATIONS OF CONCENTRATED WEIGHTS FOR

VIBRATIONAL ANALYSIS

Component	Node Location	Weight, lbs *
IPPE CPU	1141	4.834
MGI Canisters	1116	11.802
MGI Canisters	1161	5.269
RFF Center Piece	1	6.27
RFF Cylinder	64	6.30
Camera	185	1.94
Pump	199	1.33
Mirror	330	0.73
Bubble Sensor	110	0.52
Ultrasonics	105	0.52
RFF CPU	138	2.26
Battery Box	122-181	64.5
X-Cells	1119	6.0
X-Cells	1169	6.0

* All weights applied in the x, y, and z axis directions.

APPENDIX E

MODIFICATION OF IMAGES-3D MODEL

FOR STRUCTURAL ANALYSIS

1

APPENDIX E

MODIFICATION OF IMAGES-3D MODEL FOR ISS STRUCTURAL ANALYSIS

The vibrational analysis in Chapter 3 incorporated the use of concentrated weights located at nodes which exactly represent the weights and approximate locations of the center of mass for various experiments and the battery box. Unfortunately, concentrated weights are inactive in the static analysis routine. Beam elements were chosen to represent the battery box and experiments. Beam elements allow the simulation of a concentrated weight by adjusting three properties of the element; density, area, and length. Of these three properties concentration was given to adjusting the density of the element as density does not effect the element stiffness. Table E.1 lists the component, beam numbers, cross-sectional property and material property numbers, and weight used in the beam modeling method.

The weight of the battery box was represented by 60 beam elements. These elements are attached circumferentially to the nodes at the outer edge of the mid-plate. Each beam element represents a section of the wall, thus incorporating the stiffness of the battery box into the entire ISS. Each beam element has a frontal area of 0.704 inches and a length of 1.0341 inches. Knowing the total weight of the battery box to be 64.5 lbs., the density of each beam element was calculated to be 1.4767 lb/in³, or 1.075 lb/beam.

The Micro-gravity ignition canisters are represented by two beam elements, each

of which represent the top and bottom plates of 2 canister lumped at the tri-wall. These plates add stiffness locally to the tri-walls. The weight of two canisters is 11.802 lbs. The vibrational analysis used only the weight of two MGI plates at each beam element. An additional concentrated weight was added at the node nearest the center c^f mass to represent the mass not accounted for in the beam elements (See Appendix D). The structural analysis adjusted the density of each element to resemble the weight of the two canisters distributed over the two elements.

The IPPE CPU was also modeled with a beam element. A node was off-set from the tri-wall to approximately the location of the center of mass. An element extends between this node and a node perpendicular to it on the tri-wall.

All Rotational Fluid Flow experiments were modeled in a similar manner. A node was offset .25 inches above the nodes listed in Appendix F. The node on the plate and the off-set node make up the beam elements of the RFF components listed in Table A.1. A common distance of .25 inches was selected for the center of mass of all components. This simplification eliminates the complex calculations needed to define the center of mass of the various components. The RFF fluid cylinder and camera box connections were also modeled using beam elements. The two structures are attached to both the top and bottom platform. Two beam elements were used for the fluid cylinder and one was used for the camera. The beam elements were used to accurately model the weight and stiffness of these structures.

The beam elements modeling the center shaft region of the RFF were modified to correctly model the center piece of the RFF experiment platform. This modification

C1-2.

will model the extra weight and stiffness associated within this region.

Component	Beam #'s	Material Number	Cross-Section Number	Weight (lbs)
IPPE CPU	185	13	14	4.834
Micro-g canisters	118-119	9	9	11.802
Micro-g canisters	120-121	10	9	11.802
Fluid Cylinder	182-183	7	11	3.15/ element
Camera	184	8	12	1.94
Pump	189	14	17	1.33
Mirror	190	1	18	0.73
Bubble Sensor	186	1	15	0.52
Ultrasonics	187	1	15	0.52
RFF CPU	188	1	16	2.26
RFF Shaft	1-5	11	13	0.6/ element
Battery Box	122-181	6	10	1.075/ element
X-Cells	191-192	12	10	3.0/ element
X-Cells	193-194	12	10	3.0/ element

Table E.1 Beam element characteristics.

Material #	Young's Modulus lb/in^2	Density lb/in^3	Expansion	Poisson's Ratio
1	9.9 x 10^6	.098	6.33 x 10^{-6}	.33
2	5.0 x 10^4	.098	6.33 x 10^{-6}	.33
3,4 *	-	-	-	-
5	3.7 x 10^7	.283	6.33 x 10^{-6}	.3
6	9.9 x 10^6	1.4767	6.33 x 10^{-6}	.33
7	9.9 x 10^6	.1101	6.33 x 10^{-6}	.33
8	9.9 x 10^6	.2712	6.33 x 10^{-6}	.33
9	9.9 x 10^6	.1771	6.33 x 10^{-6}	.33
10	9.9 x 10^6	.1771	6.33 x 10^{-6}	.33
11	9.9 x 10^6	.1180	6.33 x 10^{-6}	.33
12	9.9 x 10^6	2.3974	6.33 x 10^{-6}	.3
13	9.9 x 10^6	.2032	6.33 x 10^{-6}	.33
14	9.9 x 10^6	.08	6.33 x 10^{-6}	.33

* Material properties 3 and 4 were deleted from the model.

Table E.2 Material properties.

Cross-Sect #	Area in^2	I_{yy} in^4	I_{zz} in^4	Torsional Constant(J) in^4
1	3.1416	1.669	1.669	3.3379
2	3.14	61.25	61.25	53.41
3	0.314	6.125	6.125	5.314
4-6 *	-	-	-	-
7	1.7671	1.1321	1.1321	2.2642
8	1.3744	0.5369	0.5369	1.0738
9	6.25	0.2035	52.0	52.0
10	0.704	1.8598	0.000916	1.8598
11	5.25	12.05	0.4375	12.05
12	1.3125	3.015	0.00068	3.015
13	4.6504	8.099	8.099	16.19
14	120.3	12.0	12.0	12.0
15	21.22	12.0	12.0	12.0
16	92.0	12.0	12.0	12.0
17	65.0	12.0	12.0	12.0
18	29.8	12.0	12.0	12.0

* Cross-Sectional properties deleted from model.

Table E.3 Cross-sectional Properties

APPENDIX F

ANALYSIS OF EXPERIMENT CONNECTIONS

APPENDIX F

ANALYSIS OF EXPERIMENT CONNECTIONS

Methodology

The first step in this analysis is to determine a generic distribution of forces acting on an unspecified bolt. Then each individual bolt can be analyzed for structural integrity using its particular orientation. Finally margins of safety can be calculated for each bolt in the analysis.

1. Determine the forces on each bolt assuming static equilibrium.

The forces on each bolt are determined by modeling each experiment as a box. Static analysis was performed for the general case, allowing substitution for the parameters of each experiment. To account for the orientation of each experiment in the GASCan, a rotation in the XY plane must be performed on the axial external loadings.

$$F_{x'} = F_x \cos\theta - F_y \sin\theta$$

$$F_{y'} = F_x \sin\theta + F_y \cos\theta$$

where $F_{x'}$ is the equivalent force parallel to the flange on which the experiment is mounted and $F_{y'}$ is the force normal to the flange.
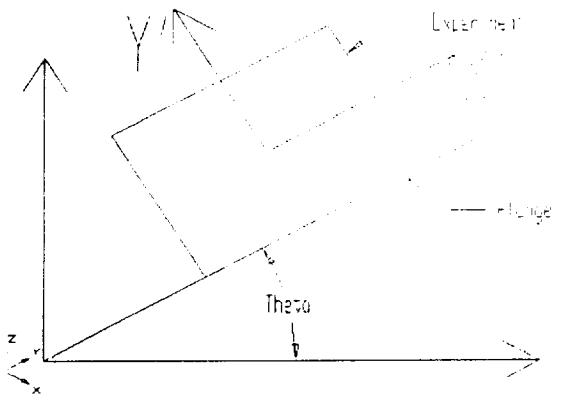
Figure F.1 Rotation terminology.

Each experiment is fastened by four bolts. For this analysis the bolts are labeled as shown to the right.
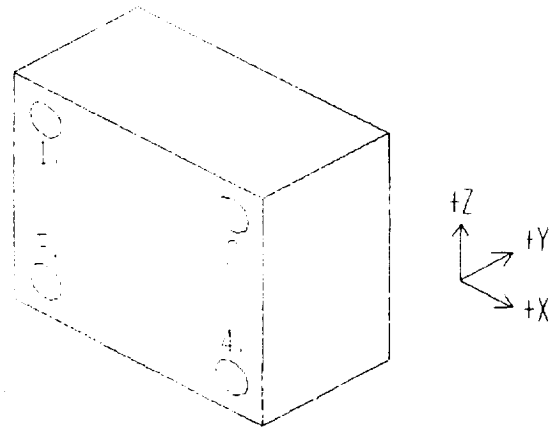
Figure F.2 Fastener configuration.

Assuming static equilibrium, the forces on each bolt (F_1, F_2, F_3 and F_4) are determined using the following equations.

3

Figure F.3 X' loading.

$$\Sigma M = 0$$
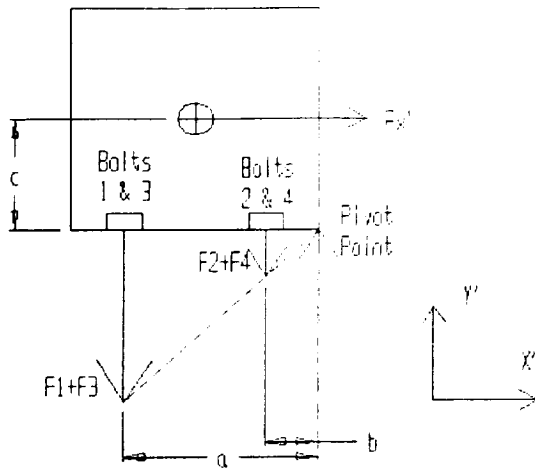
$$c(F_X) = a(F_1 + F_3) + b(F_2 + F_4)$$

Assuming also that the box is a rigid body, there is a linear relationship between the magnitude of force and the pivot point.

From trigonometry we have the equation below.

$$\frac{1}{a}(F_1 + F_3) = \frac{1}{b}(F_2 + F_4)$$

Since F_1 and F_3 are equidistant from the point of application of the load, the reaction force is divided equally between the two bolts. The same goes for F_2 and F_4. Therefore, we know that F_1 is equal to F_3 and F_2 is equal to F_4. Solving for the forces in terms of a, b, c and F_X. yields the following.

$$F_1 = F_3 = \frac{ac}{2(a^2 + b^2)} F_{X'}$$

$$F_2 = F_4 = \frac{bc}{2(a^2 + b^2)} F_{X'}$$

4

These forces act in tension on the bolts. For shear forces due to X' loading, the applied external force is divided evenly among the four bolts in the X' direction, as shown below.

$$F_{1S} = F_{2S} = F_{3S} = F_{4S} = \frac{1}{4} F_{X'}$$

Y' AXIS LOADING

Assuming static equilibrium, the forces on each bolt (F_1, F_2, F_3 and F_4) are determined using the following equations.

$$F_{Y'} + F_1 + F_2 + F_3 - F_4 = 0 \qquad\qquad \Sigma F = 0$$

Since all the bolts are equidistant from the center of mass, the reaction forces must be equal. The tension forces on the bolt due to Y' loading are:

$$F_1 = F_2 = F_3 = F_4 = \frac{1}{4} F_{Y'}$$

There is no shear component in the reaction forces for the Y' loading.

Z LOADING

The analysis for Z loading is the same as that for X'. Therefore, the tension forces due to loading along the Z axis are:

Z Loading
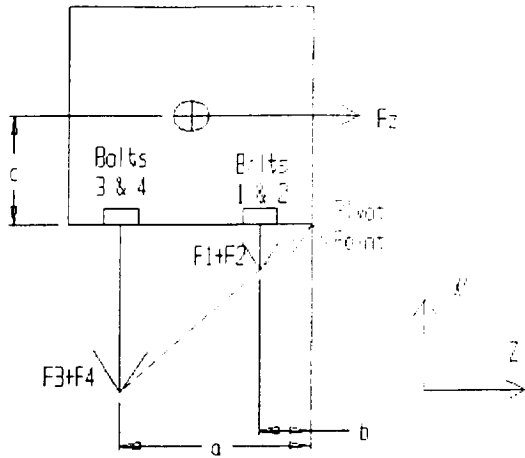
Figure F.5 Z loading.

$$F_3 = F_4 = \frac{ac}{2(a^2+b^2)} F_{z'}$$

$$F_1 = F_2 = \frac{bc}{2(a^2+b^2)} F_{z'}$$

The shear forces due to Z loading in the Z direction are:

$$F_{1S} = F_{zS} = F_{3S} = F_{4S} = \frac{1}{4} F_{z'}$$

TOTAL FORCE

Applying the convention of superposition to the X′, Y′ and Z load cases yields the total forces in shear and tension for each bolt. Since the shear components are in different directions, the magnitude of their sum is computed as follows:

$$Total\ Shear = \sqrt{(\frac{1}{4} F_{x'})^2 + (\frac{1}{4} F_{z})^2}$$

$$Total\ Shear = \sqrt{(\frac{1}{4}F_{x'})^2 + (\frac{1}{4}F_{z'})^2}$$

Analysis of Micro-Gravity Ignition Canister Mounting Bolts

Analysis of MGI Canister Mounting Bolts on Flange A

Flange A is parallel to the global X axis, therefore no rotation is needed to determine the local axis ($\Theta = 0$). Since the same four bolts fasten both canisters on either side of the flange, the analysis is performed for one can and the results are doubled. This yields the same result as performing a second analysis with a rotation angle of 180 degrees. The results are combined with the right coordination of each bolt between the analyses.

X Loading

Parameters: a = 4.0 inches   b = 1.0 inch   c = 2.5 inches

Yield case: $F_x = 109.7\ lb_f$

Ultimate case: $F_x = 146.7\ lb_f$

The resulting forces were calculated to be:

For Yield case: $F_1 = F_3 = 32.26\ lb_f$; $F_2 = F_4 = 8.07\ lb_f$; $F_s = 27.43\ lb_f$

For Ultimate case: $F_1 = F_3 = 43.15\ lb_f$; $F_2 = F_4 = 10.79\ lb_f$; $F_s = 36.67\ lb_f$

Y Loading

Parameters: Yield case: $F_Y = 29.38\ lb_f$

Ultimate case: $F_Y = 39.31\ lb_f$

The resulting forces were calculated to be:

For Yield case: $F_1 = F_2 = F_3 = F_4 = 20.07$ lb$_f$

For Ultimate case: $F_1 = F_2 = F_3 = F_4 = 26.85$ lb$_f$

Z Loading

Parameters: $a = 4.8625$ inches $b = 1.0$ inch $c = 2.5$ inches

Yield case: $F_z = 133.8$ lb$_f$

Ultimate case: $F_z = 178.4$ lb$_f$

The resulting forces were calculated to be:

For Yield case: $F_1 = F_2 = 6.79$ lb$_f$; $F_3 = F_4 = 33.0$ lb$_f$; $F_s = 33.45$ lb$_f$

For Ultimate case: $F_1 = F_2 = 9.05$ lb$_f$; $F_3 = F_4 = 44.0$ lb$_f$; $F_s = 44.6$ lb$_f$

Total External Force

Applying superposition and doubling the resultant forces from X and Z loading yields the total external tensile and shearing force on each bolt.

Bolt	F_T Yield	F_T Ultimate	F_s Yield	F_s Ultimate
1	80.84	107.8	78.0	104.0
2	45.43	60.63	78.0	104.0
3	133.26	177.7	78.0	104.0
4	97.86	130.5	78.0	104.0

Table F.1 Total external forces acting on the MGI cylinder bolts on flange A

Analysis of MGI Canister Mounting Bolts on Flange B

Flange B is rotated 60 degrees from the global X axis, therefore rotation is needed to determine the distribution of forces along the local axis. The local X and Y axes (X' and Y') are rotated -60 degrees from the global X and Y axes.

$$F_{X'} = 0.5F_X + 0.866F_Y$$

$$F_{Y'} = -0.866F_X + 0.5F_Y$$

Since the same four bolts fasten both canisters on either side of the flange, the analysis is performed for one can and the results are doubled. This yields the same result as performing a second analysis with a rotation angle of 180 degrees. The results are combined with the right coordination of each bolt between the analyses.

X' Loading

Parameters: a = 4.0 inches   b = 1.0 inch   c = 2.5 inches

   Yield case: $F_{X'}$ = 109.7 lb$_f$

   Ultimate case: $F_{X'}$ = 146.7 lb$_f$

The resulting forces were calculated to be:

For Yield case: $F_1 = F_3$ = 32.26 lb$_f$; $F_2 = F_4$ = 8.07 lb$_f$; F_s = 27.43 lb$_f$

For Ultimate case: $F_1 = F_3$ = 43.15 lb$_f$; $F_2 = F_4$ = 10.79 lb$_f$; F_s = 36.67 lb$_f$

Y' Loading

Parameters: Yield case: $F_{Y'}$ = 29.38 lb$_f$

   Ultimate case: $F_{Y'}$ = 39.31 lb$_f$

9

The resulting forces were calculated to be:

For Yield case: $F_1 = F_2 = F_3 = F_4 = 7.35$ lb$_f$

For Ultimate case: $F_1 = F_2 = F_3 = F_4 = 9.83$ lb$_f$

Z Loading

Parameters: $a = 4.8625$ inches $b = 1.0$ inch $c = 2.5$ inches

Yield case: $F_z = 133.8$ lb$_f$

Ultimate case: $F_z = 178.4$ lb$_f$

The resulting forces were calculated to be:

For Yield case: $F_1 = F_2 = 6.79$ lb$_f$; $F_3 = F_4 = 33.0$ lb$_f$; $F_s = 33.45$ lb$_f$

For Ultimate case: $F_1 = F_2 = 9.05$ lb$_f$; $F_3 = F_4 = 44.0$ lb$_f$; $F_s = 44.6$ lb$_f$

Total External Force

Applying superposition and doubling the resultant forces from X and Z loading yields the total external tensile and shearing force on each bolt.

Bolt	F_T Yield	F_T Ultimate	F_s Yield	F_s Ultimate
1	85.39	113.8	86.5	115.3
2	37.03	49.38	86.5	115.3
3	137.80	183.7	86.5	115.3
4	89.46	119.3	86.5	115.3

Table F.2 Total external forces acting on the MGI cylinder bolts on flange B.

Analysis of IPPE Equipment Mounting Bolts on Flange C

Flange C is rotated 240 degrees from the global X axis, therefore rotation is

needed to determine the distribution of forces along the local axis. The local X and Y axes (X' and Y') are rotated 240 degrees from the global X and Y axes.

$$F_{X'} = -0.5 F_X - 0.866 F_Y$$

$$F_{Y'} = 0.866 F_X - 0.5 F_Y$$

Analysis of IPPE Receiver mounting bolts on Flange C

X' Loading

Parameters: a = 2.864 inches   b = 0.325 inch   c = 1.123 inches

Yield case: $F_{X'}$ = 25.82 lb$_f$

Ultimate case: $F_{X'}$ = 34.42 lb$_f$

The resulting forces were calculated to be:

For Yield case: $F_1 = F_3$ = 4.99 lb$_f$; $F_2 = F_4$ = 0.06 lb$_f$; F_s = 6.46 lb$_f$

For Ultimate case: $F_1 = F_3$ = 6.66 lb$_f$; $F_2 = F_4$ = 0.08 lb$_f$; F_s = 8.60 lb$_f$

Y' Loading

Parameters: Yield case: $F_{Y'}$ = 6.92 lb$_f$

Ultimate case: $F_{Y'}$ = 9.22 lb$_f$

The resulting forces were calculated to be:

For Yield case: $F_1 = F_2 = F_3 = F_4$ = 1.73 lb$_f$

For Ultimate case: $F_1 = F_2 = F_3 = F_4$ = 2.31 lb$_f$

11

Z Loading

Parameters: a = 2.944 inches   b = 0.325 inch   c = 1.123 inches

Yield case: F_z = 31.5 lb$_f$

Ultimate case: F_z = 42.0 lb$_f$

The resulting forces were calculated to be:

For Yield case: $F_1 = F_2$ = 0.66 lb$_f$; $F_3 = F_4$ = 5.94 lb$_f$; F_s = 7.88 lb$_f$

For Ultimate case: $F_1 = F_2$ = 0.87 lb$_f$; $F_3 = F_4$ = 7.91 lb$_f$; F_s = 10.5 lb$_f$

Total External Force

Applying superposition and doubling the resultant forces from X and Z loading yields the total external tensile and shearing force on each bolt.

Bolt	F_T Yield	F_T Ultimate	F_s Yield	F_s Ultimate
1	7.38	9.84	14.34	19.12
2	2.45	3.27	14.34	19.12
3	12.66	16.88	14.34	19.12
4	7.73	10.31	14.34	19.12

Table F.3 Total external forces acting on the IPPE electrometer bolts on flange C.

Analysis of IPPE Electrometer Mounting Bolts on Flange C

X' Loading

Parameters: a = 2.864 inches   b = 0.325 inch   c = 1.123 inches

Yield case: $F_{x'}$ = 25.82 lb$_f$

Ultimate case: $F_{x'}$ = 34.42 lb$_f$

The resulting forces were calculated to be:

12

For Yield case: $F_1 = F_3 = 4.99$ lb$_f$; $F_2 = F_4 = 0.06$ lb$_f$; $F_s = 6.46$ lb$_f$

For Ultimate case: $F_1 = F_3 = 6.66$ lb$_f$; $F_2 = F_4 = 0.08$ lb$_f$; $F_s = 8.60$ lb$_f$

Y' Loading

Parameters: Yield case: $F_{Y'} = 6.92$ lb$_f$

Ultimate case: $F_{Y'} = 9.22$ lb$_f$

The resulting forces were calculated to be:

For Yield case: $F_1 = F_2 = F_3 = F_4 = 1.73$ lb$_f$

For Ultimate case: $F_1 = F_2 = F_3 = F_4 = 2.31$ lb$_f$

Z Loading

Parameters: $a = 2.944$ inches $b = 0.325$ inch $c = 1.123$ inches

Yield case: $F_z = 31.5$ lb$_f$

Ultimate case: $F_z = 42.0$ lb$_f$

The resulting forces were calculated to be:

For Yield case: $F_1 = F_2 = 0.66$ lb$_f$; $F_3 = F_4 = 5.94$ lb$_f$; $F_s = 7.88$ lb$_f$

For Ultimate case: $F_1 = F_2 = 0.87$ lb$_f$; $F_3 = F_4 = 7.91$ lb$_f$; $F_s = 10.5$ lb$_f$

Total External Force

Applying superposition and doubling the resultant forces from X and Z loading yields the total external tensile and shearing force on each bolt.

Bolt	F_T Yield	F_T Ultimate	F_s Yield	F_s Ultimate
1	7.38	9.84	14.34	19.12
2	2.45	3.27	14.34	19.12
3	12.66	16.88	14.34	19.12
4	7.73	10.31	14.34	19.12

Table F.4 Total external forces acting on the IPPE electrometer mounting bolts.

Analysis of IPPE CPU Mounting Bolts on Flange C

X' Loading

Parameters: a = 4.863 inches   b = 0.325 inch   c = 2.722 inches

Yield case: $F_{x'}$ = 59.38 lb_f

Ultimate case: $F_{x'}$ = 79.17 lb_f

The resulting forces were calculated to be:

For Yield case: $F_1 = F_3 = 16.54\ lb_f$; $F_2 = F_4 = 1.11\ lb_f$; $F_s = 14.85\ lb_f$

For Ultimate case: $F_1 = F_3 = 22.05\ lb_f$; $F_2 = F_4 = 1.47\ lb_f$; $F_s = 19.79\ lb_f$

Y' Loading

Parameters: Yield case: $F_{Y'}$ = 15.91 lb_f

Ultimate case: $F_{Y'}$ = 21.21 lb_f

The resulting forces were calculated to be:

For Yield case: $F_1 = F_2 = F_3 = F_4 = 3.98\ lb_f$

For Ultimate case: $F_1 = F_2 = F_3 = F_4 = 5.30\ lb_f$

Z Loading

Parameters: a = 4.872 inches   b = 0.325 inch   c = 2.722 inches

Yield case: F_x = 72.45 lb_f

Ultimate case: F_x = 96.60 lb_f

The resulting forces were calculated to be:

For Yield case: $F_1 = F_2$ = 1.35 lb_f; $F_3 = F_4$ = 20.15 lb_f; F_s = 18.11 lb_f

For Ultimate case: $F_1 = F_2$ = 1.80 lb_f; $F_3 = F_4$ = 26.87 lb_f; F_s = 24.15 lb_f

Total External Force

Applying superposition and doubling the resultant forces from X and Z loading yields the total external tensile and shearing force on each bolt.

Bolt	F_T Yield	F_T Ultimate	F_s Yield	F_s Ultimate
1	21.87	29.16	78.0	104.0
2	6.44	8.59	78.0	104.0
3	40.67	54.22	78.0	104.0
4	25.24	33.65	78.0	104.0

Table F.5 Total external forces acting on the IPPE CPU bolts.

2. Determine preload requirements for each joint

Using the highest shear and tensile forces from Step 1, along with the bolt analysis procedure detailed in Appendix H, the bolt preloads were determined.

Connection of MGI Canisters to Flanges A and B

Parameters: $K_b = 1.474 \times 10^6$ $K_j = 0.541 \times 10^6$

From equations 4 and 5: $F_p = 300\ lb_f$

Connection of IPPE Equipment to Flange C

Parameters: $K_b = 0.378 \times 10^6$ $K_j = 0.204 \times 10^6$

From equations 4 and 5: $F_p = 150\ lb_f$

3. Determine Margins of Safety for each bolt

The total force on each bolt is calculated from the external loads and preload as detailed in Appendix H. Margins of safety are then computed using equations 6 and 7 of Appendix H. The margins of safety are tabulated in Chapter 5.

Parameters for calculating margins of safety for MGI canister connection [12]

$F_{ty} = 2194.2\ lb_f$ $F_{sy} = 1206.8\ lb_f$

$F_{ty} = 3943.2\ lb_f$ $F_{sy} = 2098.8\ lb_f$

The margins of safety are tabulated in section 7.2.

Parameters for calculating margins of safety for IPPE Equipment connection [12]

$F_{ty} = 966.0\ lb_f$ $F_{sy} = 664.1\ lb_f$

$F_{ty} = 1736.0\ lb_f$ $F_{sy} = 924\ lb_f$

APPENDIX G

ANALYSIS OF WELDS

APPENDIX G

METHODOLOGY FOR THE STRESS ANALYSIS OF WELDS

The analysis of the ISS welds, which connect the tri-wall flanges to the center shaft, was a three step process. The first step is to determine the distribution of forces acting on each weld in shear and tension. The second step involves using the IMAGES-3D commercial software package to determine the maximum stress in each welded joint. Finally, the margins of safety of each weld can be determined from the forces on each weld in shear and tension.

1. Determine the forces acting on each weld in shear and tension.

The forces on each weld were determined from the forces acting on the center shaft as given by the FEM stress analysis from the IMAGES-3D commercial software package. These forces can be broken into shear and tensile force components on each flange.
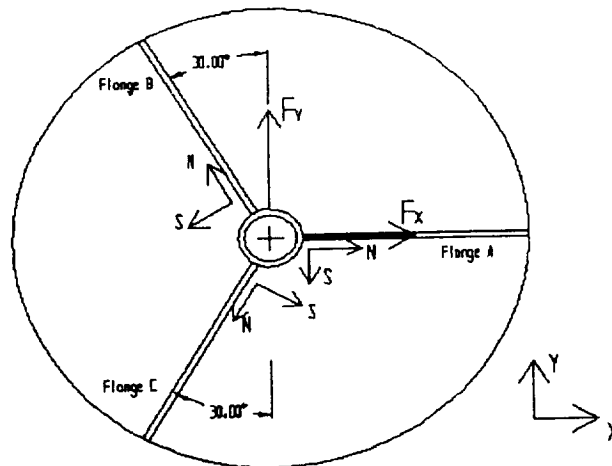
Figure G.1 Directions of forces on tri-wall welds.

2

The force on the center shaft in the Z-direction results in shear in all of the welds. The forces acting on Flange A, Flange B and Flange C in the Normal (tension) and Shear directions, as shown in Figure G.1, are distributed according to the following relations.

$$\textit{Flange A:} \quad \textit{Normal}(N) = F_X \quad \textit{Shear}(S) = F_Y$$

$$\textit{Flange B:} \quad \textit{Normal}(N) = -F_X\sin 30 + F_Y\cos 30 \quad \textit{Shear}(S) = -F_X\cos 30 - F_Y\sin 30$$

$$\textit{Flange C:} \quad \textit{Normal}(N) = -F_X\sin 30 - F_Y\cos 30 \quad \textit{Shear}(S) = F_X\cos 30 - F_Y\sin 30$$

2. Determine the maximum values of forces acting on each weld.

The forces on the center of each intermittent weld was computed in the 1992-93 MQP, so that if the highest value for stress in the intermittent weld analysis [33] is calculated over a three inch length (the planned distance between welds) and apply that load to the continuous weld, a very conservative estimate of the structural integrity of the weld should be determined.

Flange	F_{ty} (lb$_f$)	F_{sy} (lb$_f$)	F_{tu} (lb$_f$)	F_{su} (lb$_f$)
A	209.35	97.68	279.10	130.24
B	228.78	28.96	305.04	38.61
C	192.73	-126.72	256.97	-168.96

Table G.1 Maximum forces applied to tri-wall welds

where F_{ty} = Yield Tensile Force

F_{sy} = Yield Shear Force

F_{tu} = Ultimate Tensile Force

F_{su} = Ultimate Shear Force

These values are for one inch length welds with three-sixteenth inch throat (width of weld) at three inch lengths between weld centers. Therefore, if these values are divided by three inches and by three-sixteenths one obtains an average stress that can be applied over the entire weld.

Flange	σ_{ty} (lb$_f$/in^2)	σ_{sy} (lb$_f$/in^2)	σ_{tu} (lb$_f$/in^2)	σ_{su} (lb$_f$/in^2)
A	372.18	173.65	496.18	231.54
B	406.72	51.48	542.29	68.64
C	342.63	-225.28	456.84	-300.37

Table G.2 Maximum stress in tri-wall welds.

The next step in the analysis is distributing the previously found maximum stresses over the length and width of the tri-wall fillet welds [12]. The fillet welds that are on the Integrated Support Structure are eleven inches in length and one quarter inch throat (width). These calculations are stated in Table G.3.

Flange	F_{ty} (lbf)	F_{sy} (lbf)	F_{tu} (lb$_f$)	F_{su} (lb$_f$)
A	1023.49	477.54	1364.49	636.73
B	1118.48	141.57	1491.30	188.76
C	942.23	-619.52	1256.31	-826.02

Table G.3 Maximum overall force on tri-wall welds.

3. Determine the margins of safety for each weld.

The final step in verifying the structural integrity of the tri-wall welds is to determine the margins of safety for each weld. These are found using the following equations [12].

$$M.S._y = \cfrac{1}{\sqrt{\cfrac{F_{ty}^2}{f_{ty}^2} + \cfrac{F_{sy}^2}{f_{sy}^2}}} - 1$$

$$M.S._u = \cfrac{1}{\sqrt{\cfrac{F_{tu}^2}{f_{tu}^2} + \cfrac{F_{su}^2}{f_{su}^2}}} - 1$$

These relationships can be applied using fixed values for maximum forces as follows:

f_{ty} = 3375.00 lb$_f$

f_{sy} = 1856.25 lb$_f$

f_{tu} = 3937.50 lb$_f$

f_{su} = 2165.62 lb$_f$

The solutions to the previous equations yield Table G.4. which contains values for the margins of safety of the welded joints. It should be emphasized that the tabulated margins of safety are very conservative. The first reason for this is that the stresses involved are the

5

maximum calculated stresses over a three inch length that have been applied against the entire weld. The second reason is that the throat (weld width) is at the minimum size possible.

Flange	M.S.$_{yield}$	M.S.$_{ultimate}$
A	1.515	1.200
B	1.941	1.573
C	1.298	1.011

Table G.4 Minimum margins of safety on tri-wall fillet welds.

These values show that even the most severely stressed weld on the tri-wall has a margin of safety greater than one. These values indicate that the Integrated Support Structure welded joints would still be safe under loads of twice the magnitude than those that the Integrated Support Structure is expected to encounter during flight.

APPENDIX H

METHODOLOGY FOR BOLT ANALYSIS

APPENDIX H

METHODOLOGY FOR BOLT ANALYSIS

After the shear and tension reaction forces acting on each load-bearing fastener were determined the margin of safety for each fastener is individually determined by using the procedure defined in this appendix. References used in defining the formulas and methodology are NASA Systems Engineering Division's Bolted Joint Handbook [13] and Shigley's Mechanical Engineering Design [12].

The analysis procedure is relatively simple and involves a minimum number of equations. The first step is to determine the minimum fastener pre-load and then the maximum allowable fastener pre-load for each connection. The next step is to determine the margins of safety for the joint fasteners. Finally, the torque specifications are found for each fastener.

Rather than examine each fastener connection individually, each set of similar connections can be examined as a group. This is done by using the highest loadings in shear and tension for a given joint so that all fasteners will have the same pre-load and the margins of safety in the joint will not be exceeded.

1. Determine the minimum fastener pre-load for the joint.

The minimum pre-load for the fastener is one that produces a no slip, no gap condition. This condition requires that shear forces at the joint be resisted by friction forces between the fastened parts, and tensile forces be resisted by compressive forces of the joint that result from

a tensile pre-load in the fastener. The friction force must equal the external shear load and is given by:

$$Friction = \mu \, [F_P - \frac{K_J}{K_J + K_B} F_{TE}] = F_{SE}$$

where: F_{SE} = external shear load (lb$_f$)

μ = coefficient of friction at joint (dimensionless)

F_P = fastener pre-load (lb$_f$)

F_{TE} = external tensile load (lb$_f$)

K_B = bolt stiffness (lb$_f$/in)

K_J = joint stiffness (lb$_f$/in)

The bolt stiffness and joint stiffness, K_B and K_J, are calculated from:

$$K_B = \frac{E_B A_B}{L}$$

$$K_J = \frac{E_J A_C}{T}$$

where: E_B = modulus of elasticity for bolt material (psi)

E_J = modulus of elasticity for joint material (psi)

A_B = cross-sectional area of the bolt (in^2)

A_C = cross-sectional area of the joint-equivalent-cylinder (in^2)

3

L = grip length of the bolt (in)

T = grip thickness of the fastened parts (in)

The cross sectional area, A_c, is calculated from either Equation (2.4), (2.5), or (2.6) in NASA's Bolted Joint Handbook [13]. The minimum required pre-load of each joint, F_{PMIN}, is derived from equation (1):

$$F_{PMIN} = \frac{F_{SE}}{\mu} + \frac{K_J}{K_J + K_B} F_{TE}$$

The largest loadings in shear and tension for any one fastener in the joint are used for F_{SE} and F_{TE}, respectively, for a uniform pre-load of each joint. This yields a conservative value for the minimum required pre-load.

2. Determine the maximum allowable pre-load for the joint.

The maximum allowable pre-load of a joint, F_{PMAX}, as recommended by NASA's Bolted Joint Handbook [1], is equal to 65% of the bolt yield strength.

$$F_{PMAX} = 0.65 \, F_{TY}$$

where: F_{PMAX} = maximum allowable pre-load (lb_f)

F_{TY} = tensile yield load for the bolt (lb_f)

The actual pre-load for the bolts is determined by applying a factor of safety of 1.3 to F_{pmin}, as long as F_{PMAX} is not exceeded.

3. Determine the margin of safety for joint fasteners.

4

The yield margin of safety, MS_Y, and the ultimate margin of safety, MS_U, are defined by NASA's Bolted Joint Handbook [13] as:

$$MS_Y = \frac{1}{\sqrt{(F_T/F_{TY})^2 + (F_S/F_{SY})^2}} - 1$$

$$MS_U = \frac{1}{\sqrt{(F_T/F_{TU})^2 + (F_S/F_{SU})^2}} - 1$$

where: MS_Y = margin of safety for yield load case

MS_U = margin of safety for ultimate load case

F_{TY} = tensile yield load for the bolt (lb_f)

F_{SY} = 0.55 F_{TY} (lb_f)

F_{TU} = tensile ultimate load for the bolt (lb_f)

F_{SU} = shear ultimate load for the bolt (lb_f)

and F_T and F_S are the tensile and shear loads, respectively, carried by the bolt and are calculated from the external loads and the pre-load applied to the bolt using:

$$F_T = F_P + \frac{K_B}{K_J + K_B} F_{TE}$$

$$F_S = F_{SE}$$

The value for shear load is conservative since the friction force due to pre-load would cancel the external shear load at the no slip condition used to establish the minimum required pre-load.

5

4. Determine torque specifications for joint fasteners.

Torque specifications corresponding to the fastener pre-loads are calculated using the following:

$$T = F_p K D$$

where: T   = Torque (in lb_f)

F_p   = fastener pre-load (lb_f)

K   = torque coefficient (dimensionless)

D   = nominal bolt diameter (in)

Appendix D of NASA's Bolted Joint Handbook [13] uses a torque coefficient of 0.2 for 300 series stainless steel bolts. Assuming a turn of the nut method for developing the desired pre-load, the required turn past a snug tight condition is calculated from the elongation of the bolt. From the stress to strain relation the following equation for elongation is derived:

$$\Delta L = \frac{L F_p}{E_B A_B}$$

where: ΔL = fastener elongation (in)

F_p = fastener pre-load (lb_f)

E_B = modulus of elasticity for fastener material (psi)

L   = grip length of the fastener (in)

A_B = cross sectional area of the fastener (in^2)

ANALYSIS OF MOUNTING BRACKET CONNECTIONS

APPENDIX I

ANALYSIS OF MOUNTING BRACKET CONNECTIONS

An external load N, representing the center of gravity of the ISS, is applied, along each coordinate axis, to the center of gravity of the ISS, as calculated in Appendix C. The resultant forces on the structure mounting brackets are determined by considering each axis separately and then determining the total forces using superposition principles.

X-AXIS LOADING
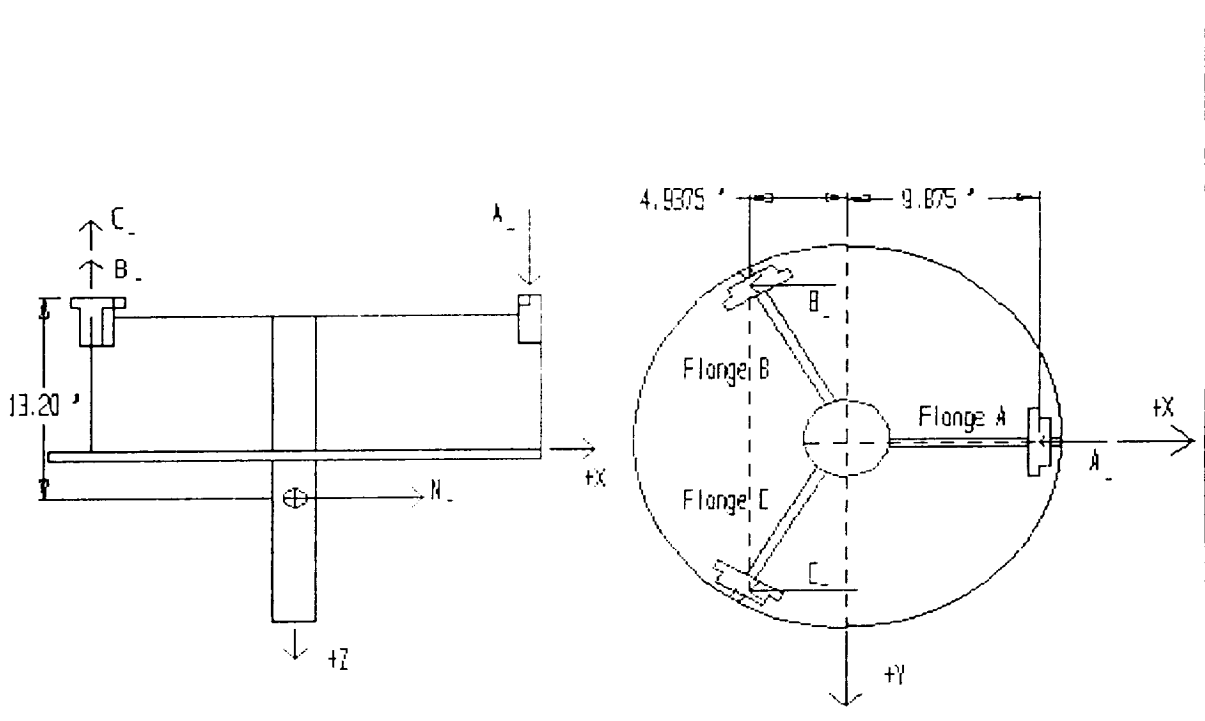
Figure I.1 X-axis loading.

The sum of all forces and moments must be zero for static

equilibrium, giving the following equations.

$$\Sigma M_x = 0, \qquad B_z + C_z = A_z$$

$$\Sigma M_y = 0 \; ; \qquad 9.875 \, A_z + 4.9375 \, (B_z + C_z) = 13.2 \, N_x$$

$$\Sigma F_z = 0; \qquad B_z = C_z$$

The solution to the previous set of equations determines the reaction forces on each bracket in the Z direction.

$$A_z = 0.9 \, N_x \qquad B_z = 0.45 \, N_x \qquad C_z = 0.45 \, N_x$$

Reaction forces in the X direction are 1/3 of the external load.

$$A_x = 0.333 \, N_x \qquad B_x = 0.333 \, N_x \qquad C_x = 0.333 \, N_x$$

Y-AXIS LOADING

For static equilibrium:

$$\Sigma M_x = 0 \; ; \qquad 13.2 \, N_y = 6.983 \, B_z + 6.983 \, C_z$$

$$\Sigma M_y = 0 \; ; \qquad 9.875 \, A_z + 4.9375 \, C_z = 4.9375 \, B_z$$

$$\Sigma F_z = 0 \; ; \qquad A_z + B_z = C_z$$

From these equations, forces in the z direction due to Y-axis loading are determined.

Reaction forces in the Y direction are 1/3 of the external

3
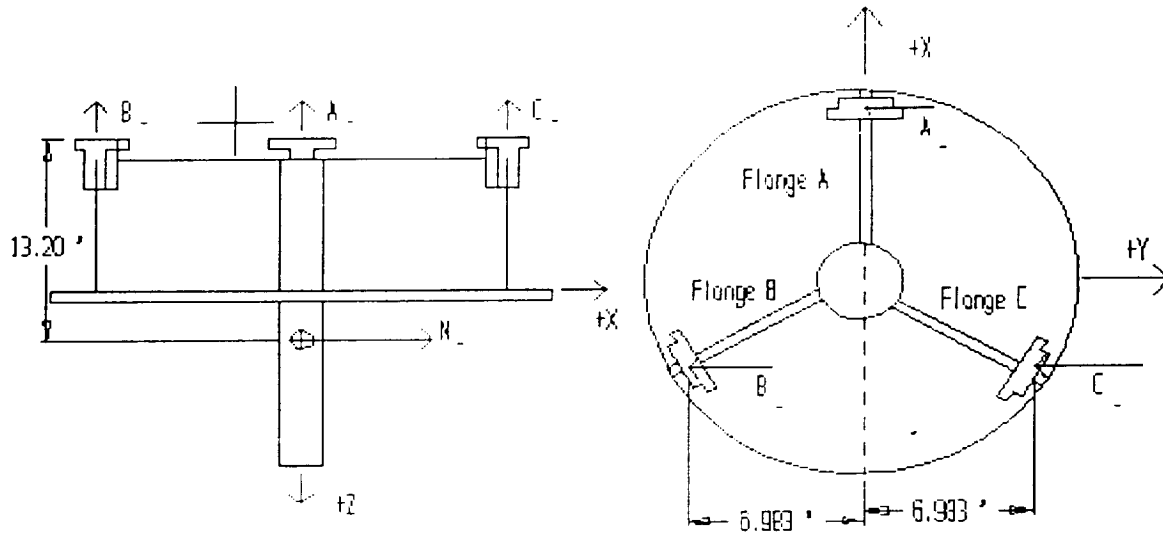
Figure I.2 Y-axis loading.

$$A_Z = 0 \qquad B_Z = -0.95 \ N_Y \qquad C_Z = 0.95 \ N_Y$$

load.

$$A_Y = 0.333 \ N_Y \qquad B_Y = 0.333 \ N_Y \qquad C_Y = 0.333 \ N_Y$$

There is no shear components in the reaction for Y′ loading.

Z-AXIS LOADING
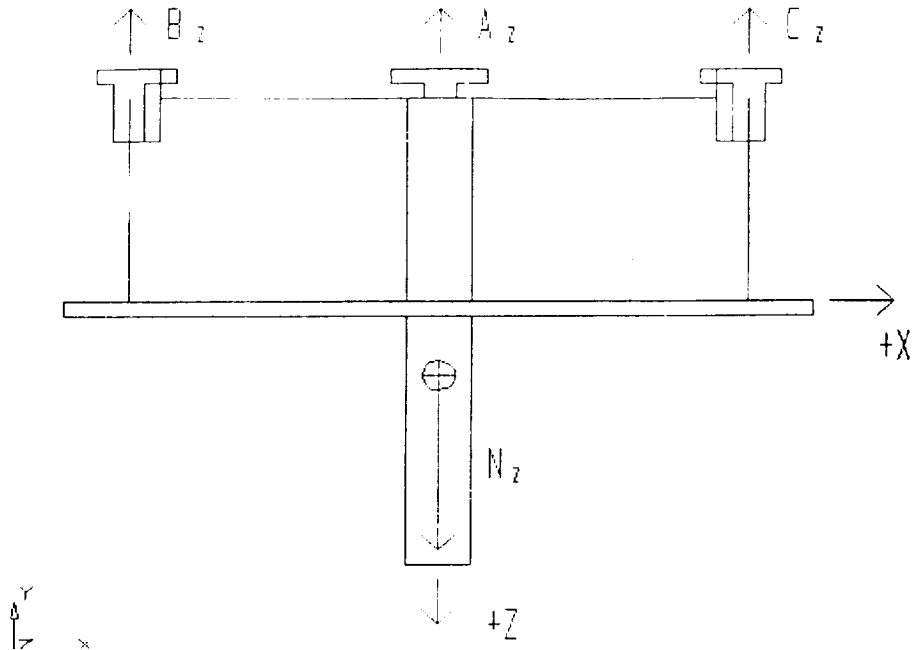
Figure I.3   Z-direction loading.

Due to the symmetry of the structure, each bracket supports 1/3 of the external load applied along the z-axis.

$$A_z + B_z + C_z + N_z = 0$$

$$A_z = -0.333 \ N_z \qquad B_z = -0.333 \ N_z \qquad C_z = -0.333 \ N_z$$

The total reaction forces on the brackets are determined by adding the forces from the three axial loadings and substituting values of N for the yield and ultimate load cases. The external forces are obtained by multiplying the total weight of the structure, as found in Appendix C, by the specified g-load along each axis.

5

Axis	Gravitational Loads		External Forces (lb$_f$)	
	Yield	Ultimate	Yield	Ultimate
X	9	12	1566	2088
Y	9	12	1566	2088
Z	15	20	2610	3480

Table I.1 G-loads and external forces applied to the mounting legs.

The reaction forces on each bracket for the yield load case are as follows:

Bracket	X (lb$_f$)	Axial Component Y (lb$_f$)	Z (lb$_f$)
A	522	522	-546.3
B	522	522	3062.3
C	522	522	86.1

Table I.2 Yield external forces applied to the mounting legs.

The reaction forces on each bracket for the ultimate load case are as follows:

Bracket	X (lb$_f$)	Axial Component Y (lb$_f$)	Z (lb$_f$)
A	696	696	-719.2
B	696	696	4083.2
C	696	696	114.8

Table I.3 Ultimate external forces applied to the mounting legs.

Analysis of Bolts Attaching Legs to the NASA Top Plate

Figure I.4 Forces acting on mounting leg bolts.
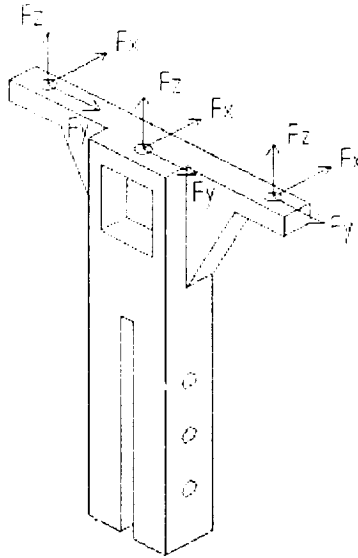
For the three bolts at the top of the structure mounting brackets, which connect the ISS to the lid of the GASCan, F_X and F_Y are shear forces, while F_Z is a tensile or compressive force on the bolt.

It is assumed that the forces applied to the brackets (A, B and C), calculated previously, are divided evenly among the three bolts. F_X and F_Y are combined to determine total shear force.

Bracket	F_{te} (lb$_f$)	F_{se} (lb$_f$)
A	-180.1	246
B	1020.8	246
C	28.7	246

Table I.4 External forces on each bolt for the yield load case.

Bracket	F_{tc} (lb$_f$)	F_{sc} (lb$_f$)
A	-239.7	328.1
B	1361.0	328.1
C	38.3	328.1

Table I.5 External forces on each bolt for the ultimate load case.

With these forces calculated, it is possible to perform the bolt analysis, as detailed in Appendix H. For 3/8-20 UN 300 series quarter hardened stainless steel bolts the following parameters were used in the calculations. [12,13]

μ = 0.45 (for aluminum on aluminum) F_{ty} = 5768.4 lb

K_b = 2.982 X 10^6 lb/in F_{tu} = 10784.4 lb

K_j = 1.944 X 10^6 lb/in F_{su} = 5517.6 lb

From equation 4 and 5 we find that F_{PMIN} = 1301.5 lb and F_{PMAX} = 3749.5 lb. A preload, F_P, of 1.3 F_{PMIN} will be used. Therefore, F_P = 1692 lb (approximately 16 ksi through the bolt). From equations 8 and 9 the total force on each bolt was calculated.

Bracket	Yield F_{ty} (lb$_f$)	Loads F_{sy} (lb$_f$)	Ultimate F_{tu} (lb$_f$)	Loads F_{su} (lb$_f$)
A	1583.0	246	1547.0	328.1
B	2309.6	246	2515.4	328.1
C	1709.2	246	1715.2	328.1

Table I.6 Total forces acting on each bolt.

8

Bracket	M.S.$_y$	M.S.$_u$
A	2.50	5.44
B	1.45	3.15
C	2.26	4.89

Table I.7 Margins of safety for each bolt.

From equation 10 and 12 we find that T = 127 in lb and θ = 0.01 degrees. The calculated torque and turn of the nut values indicate that tightening the bolt by hand with a wrench is sufficient, without specific measurements.

Fail-Safe Analysis
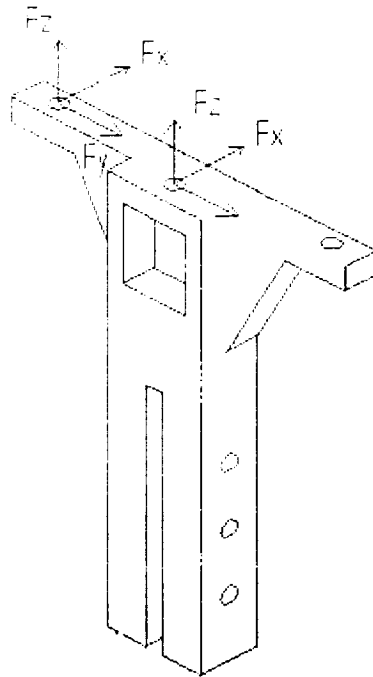
A fail-   **Figure I.5** Fail-safe
safe analysis terminology.

must be conducted where the most severely stressed bolt is removed, as if it had failed, and the joint must be reanalyzed using this

loading. With only two bolts in the bracket, each bolt will support one half of the force on the bracket. It is assumed that the moment introduced by eccentric loading is resisted by the tri-wall flange, the GASCan lid and friction in the joint.

Bracket	F_{tv} (lb$_f$)	F_{sv} (lb$_f$)	F_{tu} (lb$_f$)	F_{su} (lb$_f$)
A	-270.2	369	-359.6	492.2
B	1531.2	369	2041.5	492.2
C	43.1	369	57.5	492.2

Table I.8   Total external forces.

The total forces from equations 8 and 9, including preload, are in the following table.

Bracket	F_{tv} (lb$_f$)	F_{sv} (lb$_f$)	F_{tu} (lb$_f$)	F_{su} (lb$_f$)
A	1528.4	369	1474.5	492.2
B	2618.9	369	2927.1	492.2
C	1721.1	369	1726.8	492.2

Table I.9   Total forces including preload.

Fail-safe margins of safety can now be calculated from equations 6 and 7.

Bracket	M.S.$_Y$	M.S.$_U$
A	1.09	5.12
B	0.63	2.50
C	0.98	4.46

Table I.10   Margins of safety for failsafe analysis.

Analysis of bolts to the tri-wall flanges
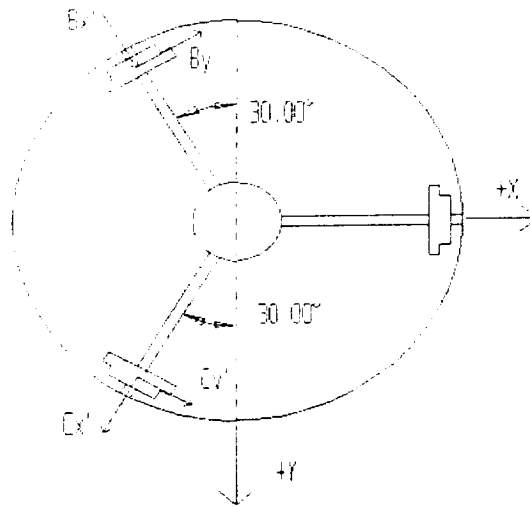
Figure I.6 Rotation
Components terminology.

of the forces in the X and Y directions were found parallel and

perpendicular to the tri-wall flanges for each bracket.

$$A_{X'} = A_X \qquad A_{Y'} = A_Y$$

$$B_{X'} = B_X \sin 30 + B_Y \cos 30$$

$$B_{Y'} = B_X \cos 30 - B_Y \sin 30$$

$$C_{X'} = -C_X \sin 30 + C_Y \cos 30$$

$$C_{Y'} = C_X \cos 30 + C_Y \sin 30$$

After performing these rotations the reaction forces on each bracket from the total ISS can be calculated.

Bracket	Yield			Ultimate		
	F_X (lb$_f$)	F_Y (lb$_f$)	F_Z (lb$_f$)	F_X (lb$_f$)	F_Y (lb$_f$)	F_Z (lb$_f$)
A	522	522	540.3	696	696	719.2
B	713.1	191.1	3062.3	950.8	254.8	4083.2
C	191.1	713.1	86.1	254.8	950.8	114.8

Table I.11   Forces on each bracket on tri-wall.

The forces perpendicular to the flange (F_Y) will be assumed to be resisted by the tri-wall flange and have negligible effect on the bolts.   In actuality, some tension will result in the bolts due to bending in the region of the joint.   The highest bending stress will occur in the flange just below the joint, however.   In addition, bolt preloads will overshadow the bolt tension that results from bending stress.
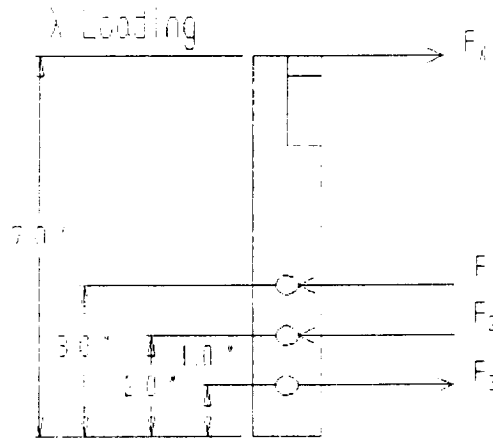
Figure I.7   X-direction loading.

12
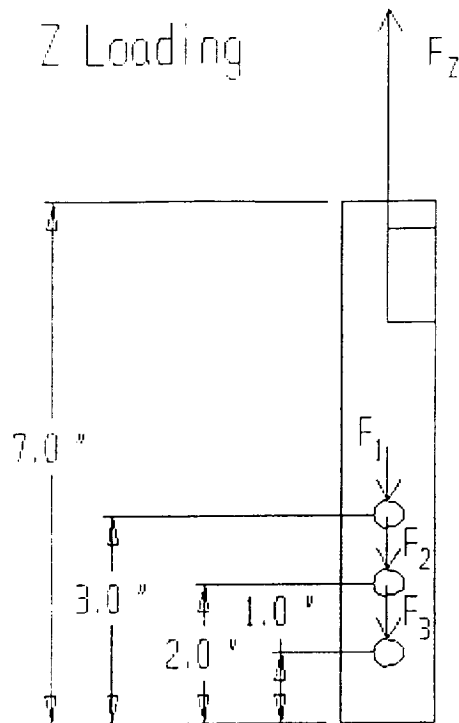
Figure I.8 Z-axis loading.

The forces on the bolts resulting from the force parallel to the flange (F_X) are calculated by assuming static equilibrium.

$$\Sigma F_X = 0; \quad F_X + F_3 = F_1 + F_2$$

It can be assumed that $F_1 = F_3$ since both forces act equidistant from the centroid of the bolt pattern. Solving the previous equations yields:

$$F_1 = \frac{5}{2} F_X \qquad F_2 = F_X \qquad F_3 = \frac{5}{2} F_X$$

Loading in the Z directions divided evenly among the three bolts, yielding the following equation for Z directional loading.

$$F_1 = F_2 = F_3 = \frac{1}{3} F_z$$

13

Forces from X and Z direction loading and combined to determine the external shear load on each bolt for all three legs.

Flange	Bolt 1 F_{SY} (lb_f)	Bolt 1 F_{SU} (lb_f)	Bolt 2 F_{SY} (lb_f)	Bolt 2 F_{SU} (lb_f)	Bolt 3 F_{SY} (lb_f)	Bolt 3 F_{SU} (lb_f)
A	1317.4	1756.4	735.5	736.1	1317.4	1756.4
B	2054.3	2739.1	1245.2	1660.3	2054.3	2739.1
C	478.6	638.1	193.2	257.7	478.6	638.1

Table I.12   Total external shear loads.

The preload for the joint and margins of safety are calculated from the external forces on each bolt using the bolt analysis, as detailed in Appendix H.   Since the external tension force on the bolts due to bending is considered negligible, the total tensile force, F_T on each bolt is equivalent to the preload, F_P, which equals 3256 pounds.

Now the margins of safety for each bolt can be calculated. These values are in the following table.

Flange	Bolt 1 M.S.$_Y$	Bolt 1 M.S.$_U$	Bolt 2 M.S.$_Y$	Bolt 2 M.S.$_U$	Bolt 3 M.S.$_Y$	Bolt 3 M.S.$_U$
A	1.72	4.28	2.23	4.60	1.72	4.28
B	1.87	3.60	1.93	3.76	1.87	3.60
C	1.40	2.59	2.15	4.34	1.40	2.59

Table I.13   Margins of safety for each bolt.

The torque and turn of wrench angle needed to produce the required preload are determined from equations 10 through 12.   The

torque, T, equals 3256 pounds and theta, θ, equals 4 degrees.

Fail-safe Analysis of the bolts to the tri-wall flanges
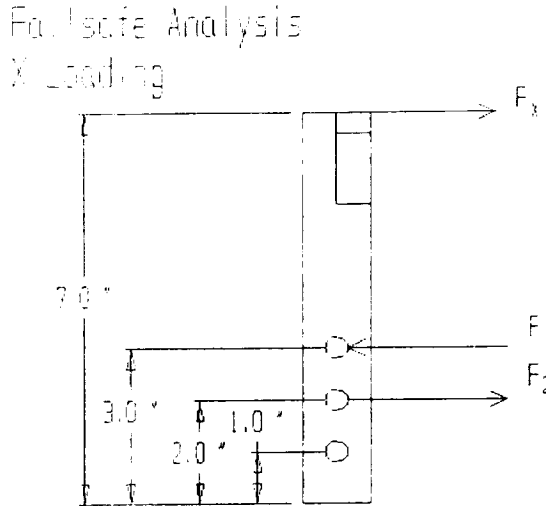
Figure I.9 X-axis failsafe
Components loading.

of the forces
in the X and Y directions were found parallel and perpendicular to
the tri-wall flanges for each bracket. After performing these
rotations the reaction forces on each bracket from the total ISS
can be calculated, as listed in Table I.14.

Bracket	Bolt 1 F_{SY} (lb_f)	Bolt 1 F_{SU} (lb_f)	Bolt 2 F_{SY} (lb_f)	Bolt 2 F_{SU} (lb_f)	Bolt 3 F_{SY} (lb_f)	Bolt 3 F_{SU} (lb_f)
A	2610	3480	2088	2784	- - -	- - -
B	3566	4754	2852	3803	- - -	- - -
C	956	1274	764	1019	- - -	- - -

Table I.14 External shear loads on bolts.

Since the external tensile force on the bolts is considered
negligible, the total tensile force on each bolt is equal to the

15

bolt preload F_p, which is equal to 3256 lb_f. Substituting the external forces into equations 6 and 7 of Appendix H yields the failsafe margins of safety.

Failsafe Analysis
Z Loading
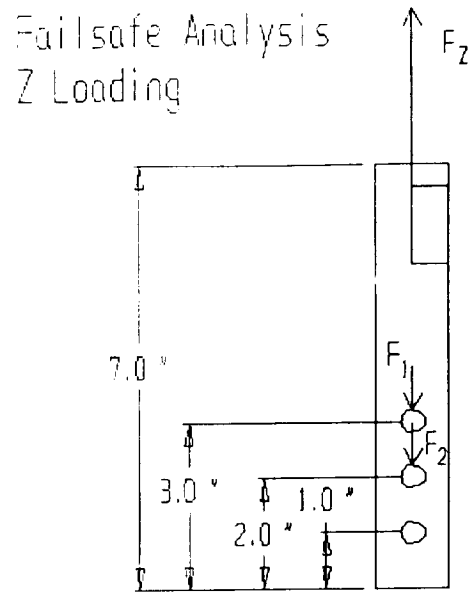
Figure I.10 Z-axis failsafe loading.

Bracket	Bolt 1 M.S.$_Y$	Bolt 1 M.S.$_U$	Bolt 2 M.S.$_Y$	Bolt 2 M.S.$_U$	Bolt 3 M.S.$_Y$	Bolt 3 M.S.$_U$
A	0.91	1.70	1.20	2.20	- - -	- - -
B	1.39	2.55	1.44	2.68	- - -	- - -
C	0.52	1.08	0.80	1.52	- - -	- - -

Table I.15 Margins of safety for failsafe analysis.

16

APPENDIX J

BATTERY BOX INFORMATION

D Cell
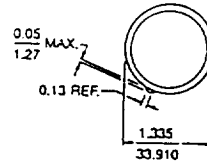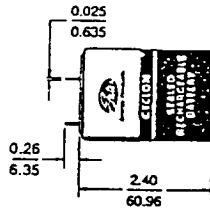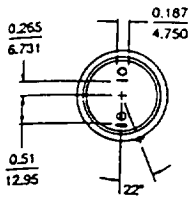
Length	2.650 in./67.31 mr
Width (dia.)	1.335 in./33.91 mr
Weight	6.4 oz./182 gm
Tabs	0.187 in. × 0.025
	4.750mm × 0.635

0.265 / 6.731   0.187 / 4.750   0.025 / 0.635   0.05 / 1.27 MAX.   0.13 REF.

0.51 / 12.95   22°   0.26 / 6.35   2.40 / 60.96   1.335 / 33.910

U.S. Patent Numbers 3,704,173-3,862,861

X Cell
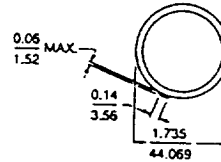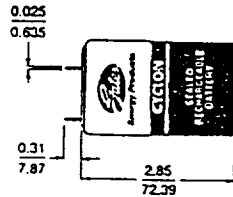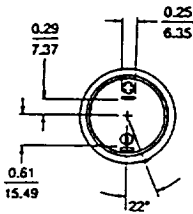
Length	3.160 in./80.26 mr
Width (dia.)	1.735 in./44.07 mr
Weight	13.0 oz./369 gm
Tabs	0.250 in. × 0.025
	6.350mm × 0.635

0.29 / 7.37   0.25 / 6.35   0.025 / 0.635   0.06 / 1.52 MAX.

0.61 / 15.49   22°   0.31 / 7.87   2.85 / 72.39   0.14 / 3.56   1.735 / 44.069

U.S. Patent Numbers 3,704,173-3,862,861

J Cell
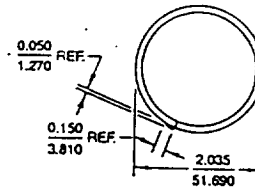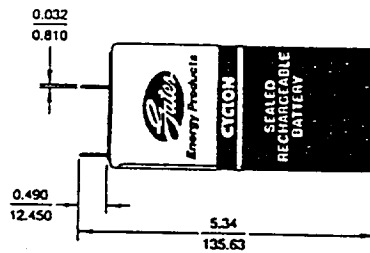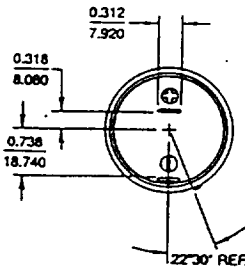
Length	5.340 in./135.63 r
Width (dia.)	2.035 in./51.69 m
Weight	1.85 lb./.84 kg
Tabs	0.312 in. × 0.032
	7.92 mm × 0.81

0.312 / 7.920   0.318 / 8.080   0.032 / 0.810   0.050 / 1.270 REF.

0.738 / 18.740   0.490 / 12.450   5.34 / 135.63   0.150 / 3.810 REF.   2.035 / 51.690

22°30' REF.

U.S. Patent Numbers 3,862,861-3,839,093

BC Cell
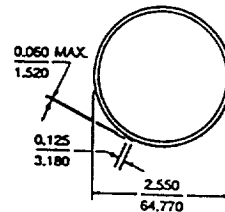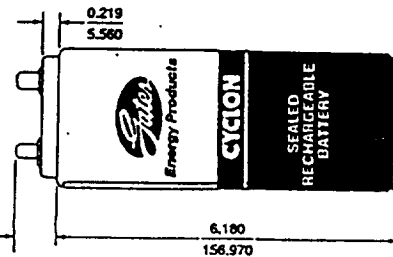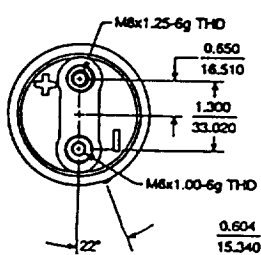
Length	6.784 in./172.31
Width (dia.)	2.550 in./64.77 m
Weight	3.490 lbs./1.58 kg
Studs	M6 × 1-6g THD
	M8 × 1.25-6G TH

Terminal torque
must not exceed
35 in. lbs. (3.95
nm)

M8x1.25-6g THD   0.219 / 5.560   0.650 / 16.510   1.300 / 33.020   0.060 MAX. / 1.520

M6x1.00-6g THD   0.604 / 15.340   6.180 / 156.970   0.125 / 3.180   2.550 / 64.770   22°

U.S. Patent Numbers 3,862,861-3,839,093

Cyclon Single Cell/Batteries Performance Specifications

Gates Energy's Cyclon cells are available in four basic sizes and may be combined to form batteries of varying sizes and capacities.

Each cell is encased in a metal can, electrically isolated to prevent accidental shorting, and incorporates a self-resealing safety valve which will vent under abusive overcharge conditions at an internal pressure of about 50psi.

Typical Specifications (Ta = 25°C)	D Cell – 2.5Ah	X Cell – 5.0Ah	J Cell – 12.5Ah	BC Cell – 2:
Product Number	0810-0004	0800-0004	0840-0004	0820-0004
Capacity Rating				
20 hour rate	2.7Ah	5.4Ah	13.0Ah	26.0Ah
10 hour rate	2.5Ah	5.0Ah	12.5Ah	25.0Ah
1 hour rate	1.8Ah	3.2Ah	9.0Ah	17.5Ah
Cell Power Rating				
Peak Power	(@135A)135W	(@200A)200W	(@350A)325W	(@600A)60(
Energy/Unit Volume (@ C/10 rate)	1.47 W-h/in³	1.48 W-h/in³	1.48 W-h/in³	1.47 W-h/in:
	0.09 W-h/cm³	0.09 W-h/cm³	0.09 W-h/cm³	0.09 W-h/cn
Energy/Unit Weight (@ C/10 rate)	12.5 W-h/lb	12.3 W-h/lb	13.5 W-h/lb	14 W-h/lb
	27.5 W-h/kg	27.17 W-h/kg	29.7 W-h/kg	31 W-h/kg
Internal Resistance (max. for a charged cell)	10 × 10⁻³ ohms	6 × 10⁻³ ohms	4 × 10⁻³ ohms	3 × 10⁻³ ohm
	Measured on Hewlett-Packard 4328A milliohm meter.			
Nominal Cell Voltage	2.0V	2.0V	2.0V	2.0V

Cell Temperature Range	Storage	−65°C to +65°C
	Discharge	−65°C to +65°C
	Charge	−40°C to +65°C

Storage Time	Ta = 0°C	7,200 days
	Ta = 23°C	1,200 days
	Ta = 65°C	60 days

Atmospheric Pressure Range	0-8 Atmospheres

Cell Charging	Constant Voltage	
	cyclic	2.40-2.60V
	float	2.30-2.40V
	Constant Current	
	cyclic, maximum	C/3 rate for D, X, J cells, C/5 rate for BC cells
	float, maximum	C/500 rate

Cycle Life	200-2,000 cycles	200 cycles — 100% depth of discharge, one cycle per day (Charge: 2.45V constant no current limit; Discharge: C/5 rate); 2000 cycles — 25% depth of discharge (Char; cell for 7.5 hrs. — 2.0A current limit; Discharge: C/2 rate for 30 min); More cycles a available with shallower discharges.

Expected Float Life	8 years	Based on accelerated test methods, 2.35 volts constant voltage charge at 23°C am! temperature.

APPENDIX K

LATERAL BUMPER DESIGN

APPENDIX K

LATERAL SUPPORT BUMPER DESIGN

MODIFICATIONS TO LATERAL SUPPORT BUMPERS

The current design of the lateral support bumper is a modification of the design from the 1992-93 MQP [33], which was based upon the lateral support bumper design used in GASCan I [5]. The bumper assembly consists of two opposing wedges and a mounting bracket. A bolt threaded down the center of the internal wedge is used for tightening the lateral bumper assembly. Safety and fail-safe analysis concerns have been addressed with the use of two nylon locking nuts countersunk and attached to the bottom of the internal wedge. This ensures that the bolt will not loosen due to the structural and vibrational loads encountered during the mission.

INTERNAL WEDGE

The internal wedge has been modified to match the angle of the bumper body. This allows for greater bumper travel and addresses spacial concerns as well. While the nylon locking nuts are used for safety precautions, the internal wedge will be constructed of stainless steel to prevent possible stripping of the threads in the internal wedge.

BODY-PAD SURFACE

The surface area of the wedge is five square inches, one square inch over the NASA prescribed minimum of four square inches per bumper. The mating wedge angle has been altered to an angle of 30 degrees from the vertical, from the GASCan I design angle of 17

2

degrees. The greatest movement this design should need to move is slightly over .125 inches, but this design can move approximately .177 inches. This number almost triples the movement of the GASCan I lateral support bumper design.

MOUNTING

The three lateral bumper assemblies will be attached to the bottom of the sides of the battery box using mounting brackets similar to the ones used in GASCan I. The lateral bumper body will be slide-pinned, using a 1/8" pin, to the mounting bracket with the internal wedge sandwiched between. The pin-slide slots in the sides of the lateral bumpers prevent any movement except in the lateral direction. They were given a larger lateral size to allow the bumper greater travel. The 3/8" stainless steel bolt for securing the bumper assembly is threaded through the internal wedge and then through two nylon locking nuts which are countersunk into the bottom of the internal wedge. There are two nylon locking nuts for safety and fail-safe requirements.

MODIFICATIONS TO VITON MOUNTING PROCEDURE [33]

The Viton strip was previously mounted to a polished aluminum surface. A silicon adhesive was used to hold the Viton onto the aluminum. This connection proved to be very poor. A new method for adhering the Viton to the aluminum surface is employed. First, the aluminum surface is a rough etched surface, not polished. Second, a new manufacturer was located that produces their own adhesive to bond their particular Viton product to metal surfaces.

3

APPENDIX L

LATERAL BUMPER STIFFNESS DETERMINATION

APPENDIX L

LATERAL BUMPER STIFFNESS DETERMINATION

Methodology

A finite element model of an ISS later bumper was constructed to determine its equivalent spring stiffness, as shown in Figure L.1. Thirty-six load cases of nodal forces were applied to the nodes at the face of contact between the bumper model and the inner diameter of the GASCan shell. For these load cases the equivalent bumper stiffness can be determined from a finite element stress analysis for the bumper by applying the linear relationship $k = F/\delta$ where F is the applied force and δ is the displacement, in the direction of F. The finite element model was constructed using ARIES Conceptstation commercial software package and the analysis was solved by MSC/NASTRAN.

Finite Element Model

This model, shown in Figure L.2, consists of 1544 nodes and 1050 brick elements. The nodes corresponding to the face of contact between the bumper bracket and the FEM bumper, an assembly of the aluminum lateral bumper and the stainless steel internal wedge, are fully constrained.

A nodal force load of 100 pounds was applied to the bumper face/GASCan shell at thirty-six nodes. The displacement of the node in each load case is used to determine the stiffness of the bumper assembly. An average stiffness ratio can be found by averaging the values of the stiffness ratios.
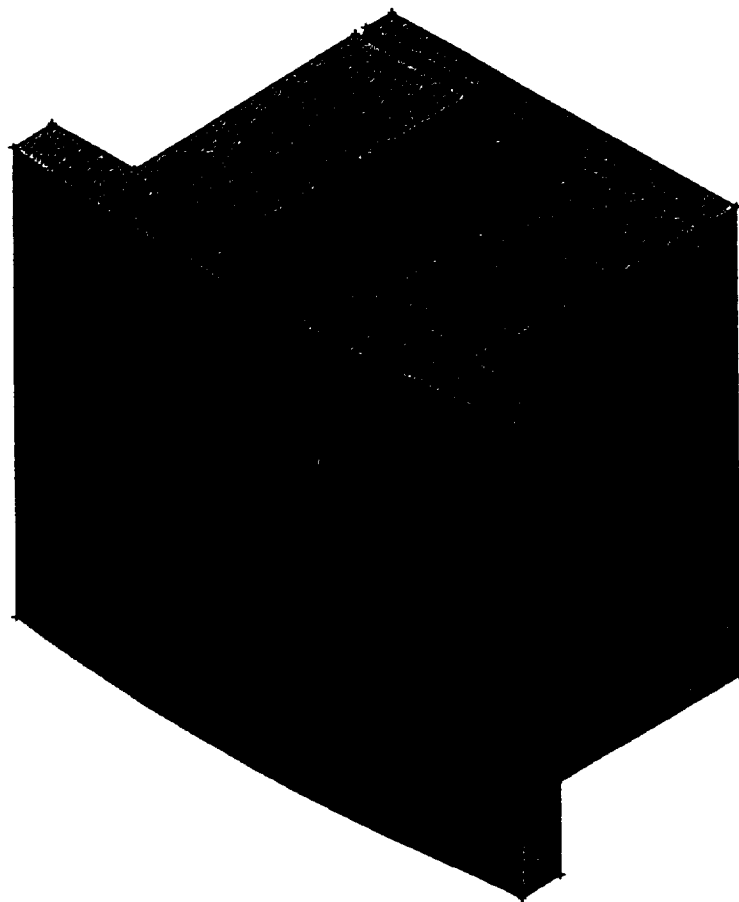
2

Figure L.1 FEM assembly drawing.

3
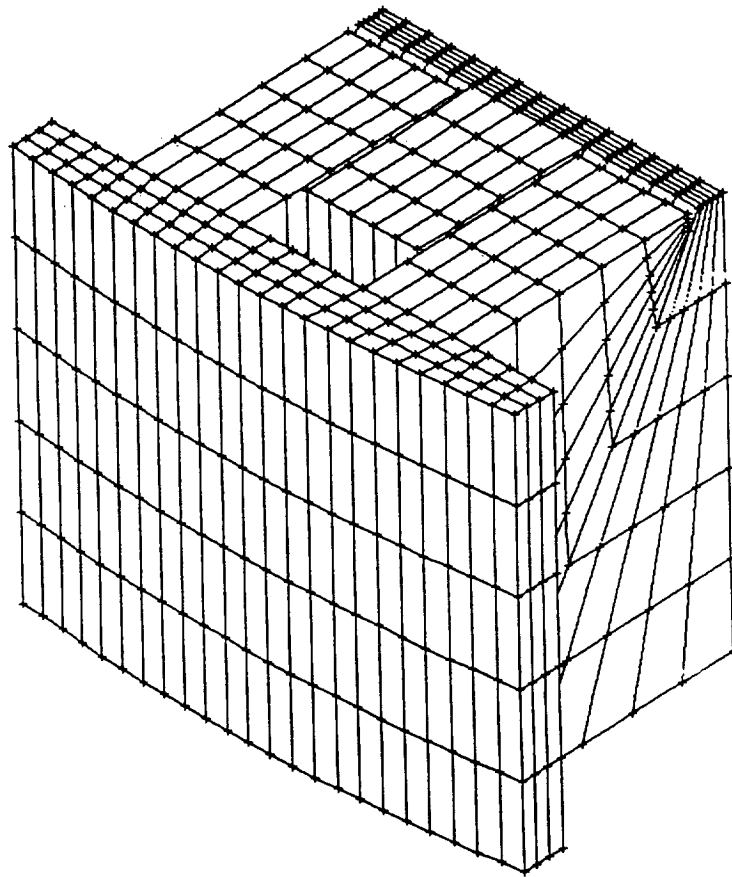
Figure L.2 FEM mesh.

RESULTS

The finite element model was used to determine the displacements occurring during a loading case. Each of these displacements are listed in the table below.

Nodes	Column 1 (10^{-3} in)	Column 2 (10^{-3} in)	Column 3 (10^{-3} in)	Column 4 (10^{-3} in)	Column 5 (10^{-3} in)	Column 6 (10^{-3} in)
Row 1	1.69837	0.615607	0.311281	0.260875	0.268614	0.324526
Row 2	0.853788	0.275091	0.133850	0.110930	0.114925	0.129173
Row 3	0.718692	0.216975	0.102843	0.086315	0.098398	0.112107
Row 4	0.697938	0.202071	0.091812	0.076994	0.084377	0.106153
Row 5	0.844378	0.247101	0.094056	0.073667	0.077107	0.100998
Row 6	1.95957	0.789058	0.341684	0.160855	0.143353	0.144016

Table L.1 Displacements encountered under 100 pound nodal load.

The spring constant for each nodal location was then found using the linear relationship $k = F/\delta$. This set of calculations gives the following table.

Nodes	Column 1 (lb/in)	Column 2 (lb/in)	Column 3 (lb/in)	Column 4 (lb/in)	Column 5 (lb/in)	Column 6 (lb/in)
Row 1	58.88 E3	162.4 E3	321.3 E3	383.3 E3	372.3 E3	308.1 E3
Row 2	117.1 E3	363.5 E3	747.1 E3	901.5 E3	870.1 E3	774.16 E3
Row 3	139.1 E3	460.9 E3	972.4 E3	1158.5 E3	1016.3 E3	892.0 E3
Row 4	143.3 E3	494.9 E3	1089.2 E3	1298.8 E3	1185.2 E3	942.0 E3
Row 5	118.4 E3	404.7 E3	1063.2 E3	1357.5 E3	1296.9 E3	990.1 E3
Row 6	51.03 E3	126.7 E3	292.67 E3	621.68 E3	697.58 E3	694.4 E3

Table L.2 Spring constants derived from linear relationship.

The average stiffness ratio can be found by averaging the spring constant values in the above table. The average stiffness ratio of the lateral bumper is $k = 6.09588 \times 10^5$ lb/in.

APPENDIX M

ANTENNA FINITE ELEMENT METHODOLOGY

APPENDIX M

ANTENNA FINITE ELEMENT METHODOLOGY

The IPPE antenna finite element model was generated in three parts. The center of the antenna top hat and its threaded connection were constructed with 24 plate elements which accurately represent the mass of the combined top hat and connection. An additional 48 plate elements represent the outer ring of the antenna top hat. The antenna shaft which consists of 12 beam elements. The same model was used for both vibrational and stress FEM analyses.

The weights and center of gravity both align themselves very well with hand calculations, to 0.2 and 0.08 percent error respectively. This agreement is a good indication of the FEM models' reliability.

COMPONENT	WEIGHT (LB)
TOP HAT AND CONNECTION	0.290
ANTENNA SHAFT	0.660

Table M.1 IPPE antenna weights.

Total   0.950 lbs
Weight returned by FEM anaylsis 0.9483 lbs
Error   0.2 %

COMPONENT	WT (lb)	X (in)	Y (in)	Z (in)
TOP HAT AND CONNECTOR	0.290	0	0	12.0
ANTENNA SHAFT	0.660	0	0	6.0

Figure M.2 tabulated coordinates for the center of mass.

HAND ANALYSIS CENTER OF MASS $\overline{X}$=0.00 $\overline{Y}$=0.00 $\overline{Z}$=7.83

FEM MODEL CENTER OF MASS $\overline{X}$=.7e⁻8 $\overline{Y}$=.2e⁻9 $\overline{Z}$=7.83

3

The hand analysis center of mass was calculated using the following equations.

$$\overline{X} = \frac{\sum (X_i \ W_i)}{\sum W_i}$$

$$\overline{Y} = \frac{\sum (Y_i \ W_i)}{\sum W_i}$$

$$\overline{Z} = \frac{\sum (Z_i \ W_i)}{\sum W_i}$$

Where X_i, Y_i, Z_i, are the respective coordinates of each component, treated as point masses, and W_i is the weight of each component. The finite element model returned values that with no more than 0.1 percent error along any Cartiesian axis.

Material #	Young's Modulus lb/in^2	Density lb/in^3	Expansion	Poisson's Ratio
1	29 x 10^6	0.28	6.33 x 10^{-6}	.27
2	29 x 10^6	0.287	6.33 x 10^{-6}	.27
3	29 x 10^6	1.113	6.33 x 10^{-6}	.27

Table E.2 Material properties.

4

The different material densities were used to correctly simulate the added weight on the connection between the antenna shaft and the top hat, and to make up for the lost volume at the edge to the circular top hat which is represented by rectanglar plates.

Cross-Sect #	Area in^2	I_{yy} in^4	I_{zz} in^4	Torsional Constant(J) in^4
1	0.19635	0.003068	0.003068	0.0061359

Table E.3 Cross-sectional Properties.

APPENDIX O

MICRO-GRAVITY IGNITION BRACKET ANALYSIS

APPENDIX O

MICRO-GRAVITY IGNITION BRACKET ANALYSIS

The bracket analysis was based upon Shigley's Mechanical Engineering Design textbook,

in the Design of Screws, Fasteners, and Connections chapter (Chapter 8) [12].

First, The thread length of inch-series bolts had to be determined:

$$l_t = 2d + 1/4$$

where d is the diameter of the bolt.

Once the bolt is selected, the stiffness constants of the threaded and unthreaded parts of

the bolts can be calculated as follows:

$$k_d = \frac{EA_d}{l_d} \qquad\qquad k_t = \frac{EA_t}{l_T}$$

where E is the modulus of elasticity for the bolts, and the two lengths are the threaded lengths

and unthreaded lengths, respectively.

Once both stiffness constants have been found, they can be combined into the effective

stiffness of the bolt in the clamped condition:

2

P_m, the portion of P taken by the members;

$F_b = P_b + F_i$, the resultant bolt load;

$F_m = P_m - F_i$, the resultant load on members;

$$F_b = \frac{k_b P}{k_b + k_m} + F_i$$

$$F_m = \frac{k_m P}{k_b + k_m} - F_i$$

From this, the coefficient C can be derived:

$$C = \frac{k_b}{k_b + k_m}$$

STRESS FACTORS

Now that the variables have been defined, the behavior of the bolt can be studied under

static loading. The tensile stress in the bolt is:

$$\sigma_b = \frac{CP}{A_t} + \frac{F_i}{A_t}$$

Using this data, safety factors can be determined:

LOAD FACTOR, n_1

(Prevents separation):

$$n_1 = \frac{F_i}{P(1-C)}$$

Once static loading has been accounted for, fatigue loading has to be studied for safety. In fatigue loading, it is assumed that there is an alternating bolt stress, which fluctuates from the initial preload stress to the stress occurring at the maximum tensile load.

ALTERNATING STRESS:

$$\sigma_a = \frac{CP}{2A_t}$$

$$S_a = \frac{[S_{ut} - \frac{F_i}{A_t}]}{[1 + \frac{S_{ut}}{S_e}]}$$

MEAN STRESS:

5

$$\sigma_m = \frac{CP}{2A_t} + \frac{F_i}{A_t}$$

These can be used to determine other important safety factors:

FATIGUE FAILURE FACTOR OF SAFETY, n_2 :

$$n_2 = \frac{S_a}{\sigma_a}$$

YIELDING FACTOR OF SAFETY, n_3:

$$n_3 = \frac{S_y}{\sigma_m + \sigma_a}$$

BRACKET STRESS:

Once the bolt stress has been calculated, the bracket stress should be calculated as well.

For this case, the bracket geometry has been simplified for ease of calculation.

$$\sigma = \frac{P}{A}$$

This stress is equal to the load (the weight of the cylinder) divided by the area perpendicular to the load. The area can be simulated as the difference between the area of the outer and inner diameters of the bolt. Although this area is not precise, it is smaller than the actual area, yielding a conservative estimate.

SAMPLE CALCULATIONS:

The bolts should be 300 type stainless steel. For this calculation, type A307 bolts will be used (yield strength is 36 ksi).

This factor of safety has the lowest value compared to the other two.

$$n_3 = \frac{S_y}{\sigma_m + \sigma_a}$$

$$n_3 = \frac{36ksi}{.00342ksi + 14.4544kpsi}$$

$$n_3 = 2.49$$

NASA is mainly concerned with the margin of safety, which is equal to the factor of safety minus the safety requirement:

$$M.S. = 2.49 - 1.5 = .99$$

Therefore, a positive margin of safety indicates that the bolt will not fail under these loadings.

Bracket Stress:

$$\sigma = \frac{4.25lbs}{\Pi(\frac{5.5}{2})^2 - \Pi(\frac{4.5}{2})^2}$$

$$\sigma = .5408 \text{ psi}$$

8

The results for the three factors of safety for the bolts (separation, fatigue failure, and yielding) are equal to 16.727, 7.97, and 1.6. While it appears that the first two are unusually high, they are reasonable due to the low load (weight of one bracket) and high strength of the aluminum bracket and stainless steel bolts. The stress in the bracket is equal to .5408 psi. This is low for the same reasons.

The required factor of safety is 1.5 for this kind of analysis. Therefore, the bolts and brackets are well within the requirements necessary for safety. Neither the bolts nor the brackets will fail during flight.

APPENDIX P

NASA CONNECTORS

GET AWAY SPECIAL
SMALL SELF-CONTAINED PAYLOADS
ELECTRICAL INTERFACE CONNECTORS

SIGNAL CONNECTOR

J-401
DDM-50S NMB-76

Pin	Signal
3	GCD RELAY B ARM
36	GCD RELAY B HOT
20	GCD RELAY B LATENT
4	GCD RELAY C ARM
37	GCD RELAY C HOT
21	GCD RELAY C LATENT
5	PPC MALFUNCTION SENSOR 1
38	PPC MALFUNCTION SENSOR 2
22	PPC COMMON
6	PPC COMMON

DIRECT CONNECTION TO
EXTERNAL TEST CONNECTOR PINS

41, 25, 9, 42, 26, 10, 43, 27, 11, 44, 28, 12, 45, 29, 13, 46, 30, 14, 47, 31, 15, 48, 32, 16, 49, 33, 17, 50

P-401
DDM-50P-NMB 76

GCD RELAYS B AND C FOR PAYLOAD CONTROL
FROM PAYLOAD MALFUNCTION INPUTS
TO MALFUNCTION COMMON

PAYLOAD GROUND TEST LINES

POWER CONNECTOR

P-400
JT06RE-16-6S

Pin	
A	FROM PAYLOAD BATTERY CIRCUIT 1
B	FROM PAYLOAD BATTERY CIRCUIT 2
C	TO PAYLOAD POWER BUS 1
D	TO PAYLOAD POWER BUS 2
E	TO PAYLOAD POWER COMMON
F	TO PAYLOAD POWER COMMON

J-400
JT07RE-16-6P

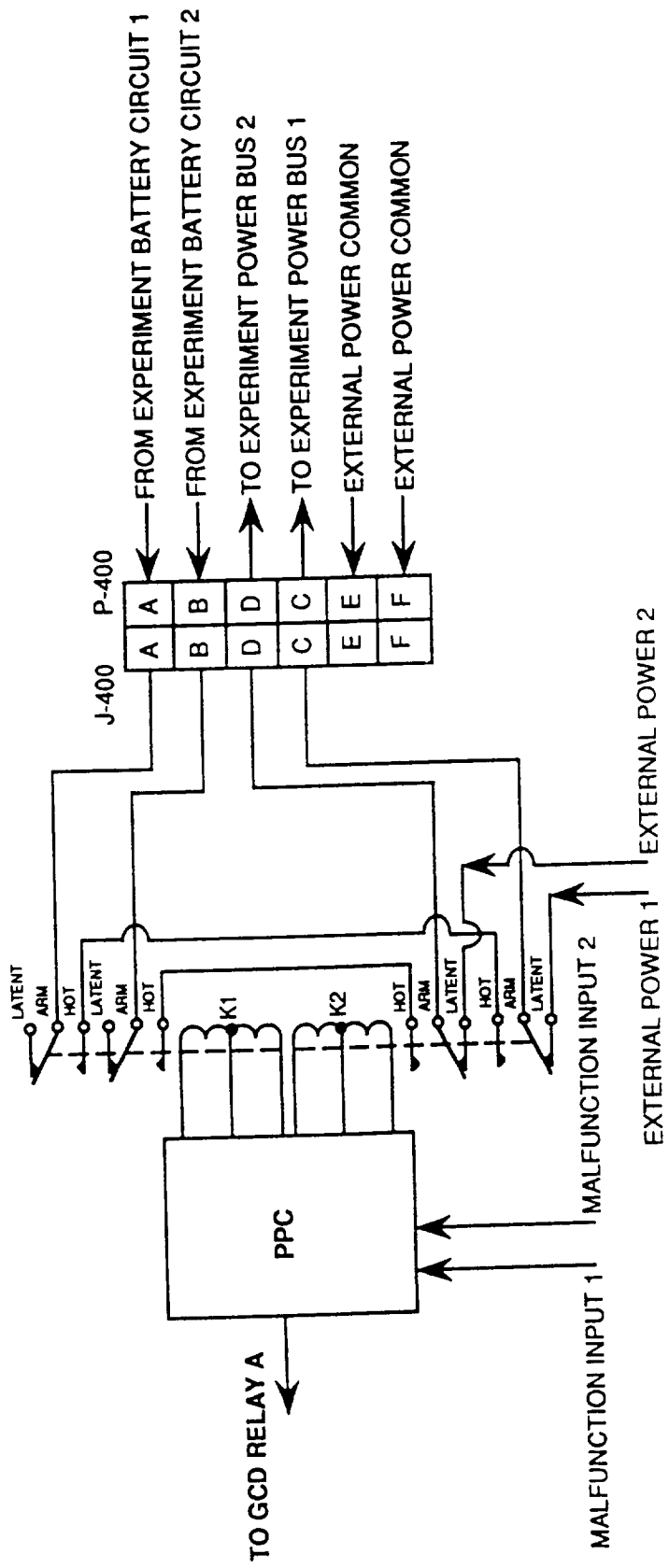| Pin	
A	TO RELAY K1
B	TO RELAY K1
C	TO RELAY K2
D	TO RELAY K2
E	EXTERNAL POWER COMMON
F	EXTERNAL POWER COMMON

PAYLOAD

NASA INTERFACE EQUIPMENT PLATE

FIGURE 2 - PAYLOAD POWER CONTACTOR (PPC)

APPENDIX Q

ENGINEERING DRAWINGS

1